

Modeling Hydrogen-Bonding in Diblock
Copolymer/Homopolymer Blends

MODELING HYDROGEN-BONDING IN DIBLOCK
COPOLYMER/HOMOPOLYMER BLENDS

BY

ASHKAN DEHGHAN, B.Sc.

A THESIS

SUBMITTED TO THE DEPARTMENT OF PHYSICS & ASTRONOMY

AND THE SCHOOL OF GRADUATE STUDIES

OF MCMASTER UNIVERSITY

IN PARTIAL FULFILMENT OF THE REQUIREMENTS

FOR THE DEGREE OF

MASTER OF SCIENCE

© Copyright by Ashkan Dehghan, September 2012

All Rights Reserved

Master of Science (2012)
(Physics & Astronomy)

McMaster University
Hamilton, Ontario, Canada

TITLE: Modeling Hydrogen-Bonding in Diblock Copolymer/Homopolymer Blends

AUTHOR: Ashkan Dehghan
B.Sc., (Theoretical Physics)
McMaster University, Hamilton, Canada

SUPERVISOR: Dr. An-Chang Shi

NUMBER OF PAGES: ix, 68

Abstract

The phase behavior of AB diblock copolymers mixed with C homopolymers (AB/C), in which A and C are capable of forming hydrogen-bonds, is examined using self-consistent field theory. The study focuses on the modeling of hydrogen-bonding in polymers. Specifically, we examine two models for the formation of hydrogen-bonds between polymer chains. The first commonly used model assumes a large attractive interaction parameter between the A/C monomers. This model reproduces correct phase transition sequences as compared with experiments, but it fails to correctly describe the change of lamellar spacing induced by the addition of the C homopolymers. The second model is based on the fact that hydrogen-bonding leads to A/C complexation. We show that the interpolymer complexation model predicts correctly the order-order phase transition sequences and the decrease of lamellar spacing for strong hydrogen-bonding. Our analysis demonstrates that hydrogen-bonding of polymers should be modeled by interpolymer complexation.

Acknowledgements

I would like take a moment and truly thank the wonderful people who helped me during my masters study. First and foremost, I would like thank my parents Fatemeh Taheri and Mehran Dehghan for supporting me and my goals, regardless of how absurd they might have been. This work would not have been possible without the support and help of my supervisor, An-Chang Shi, whose guidance is truly appreciated. I would also like to thank Kari Dalnoki-Veress for encouraging me to continue my studies at the graduate level. I am very grateful to my colleagues Jiajia Zhou and Kyle Pastor for great discussions and useful critiques over the past few years. Last but not least I would like to acknowledge the help of Sarra Saiyed with the editing of my thesis.

Contents

Abstract	iii
Acknowledgements	iv
1 Introduction	1
2 Self-Consistent Field Theory	6
2.1 Theoretical Framework	6
2.2 The Homogenous Phase	18
3 The Random Phase Approximation	21
4 Numerical Methods	28
4.1 Reciprocal-Space Method	29
4.2 Alternating Direction Implicit Method	33
5 Results and Discussion	38
5.1 The Attractive Interaction Model	39
5.2 The Interpolymer Complexation Model	49
6 Summary and Conclusion	61

List of Figures

1.1	Schematic diagram for AB/C system, where the C homopolymer is capable of hydrogen bonding with block A of the diblock copolymer.	4
2.1	Schematic diagram showing the complexation process. The prime symbols are used for bookkeeping purposes to distinguish between the A , B and C segments in the diblock copolymer, homopolymer and complexed chains.	7
2.2	Schematic diagram showing the end integrated propagators for a diblock chain.	16
5.1	Schematic diagram for AB/C complexation, where the C homopolymer is capable of hydrogen-bonding with A block of the diblock copolymer.	39
5.2	RPA phase diagram for blends with parameters $\chi_{AB} = 12, \chi_{AC} = -10, \chi_{BC} = 15$ and $\kappa = 0.5$. The 2-phase region is a macrophase separated state with diblock rich/ homopolymer rich macroscopic domains.	41
5.3	RPA phase diagram for blends with parameters $\chi_{AB} = 12, \chi_{BC} = 15, f_A = 0.5$ and $\kappa = 0.5$	42

5.4	The phase diagram for the AB/C blend with $\chi_{AC} = -10$, $\chi_{BC} = 15$, $\chi_{AB} = 12$ and $\kappa = 0.5$. Disordered, Microphase separated and two phase regions are observed. In the microphase region, Lamellar (lam), Cylindrical (Hex) and Spherical (BCC) phases are shown.	43
5.5	Phase diagram for the AB/C blend with $\chi_{AB} = 12$, $\chi_{BC} = 15$, $f_A = 0.5$ and $\kappa = 0.5$	45
5.6	Normalized lamellar spacing for the AB/C system with $\chi_{AB} = 12$, $\chi_{BC} = 15$, $f_A = 0.5$, $\kappa = 0.5$ and $\chi_{AC}=-10$ (dotted line) and $\chi_{AC}=-1$ (solid line).	46
5.7	Density profile for the AB/C system, with $\chi_{AB} = 12$, $\chi_{BC} = 15$, $f_A = 0.5$, $\kappa = 0.5$ and $\chi_{AC}=-10$ (dotted line) and $\chi_{AC}=-1$ (solid line). ϕ_H is 20% for both blends. The x axis is the axis perpendicular to the lamellar interface, normalized with respect to the lamellar domain spacing.	47
5.8	Density profile for the AB/C system, with $\chi_{AB} = 12$, $\chi_{BC} = 15$, $f_A = 0.5$, $\kappa = 0.5$ and $\chi_{AC}=-10$ (dotted line) and $\chi_{AC}=-1$ (solid line). ϕ_H is 20% for both blends.	48
5.9	Schematic diagram showing a few examples of what could result from a linear complexation. In this model, D segments are the result of the complexation of the A and C monomers.	50
5.10	Graphical representation of solutions to equation (5.30) for the AB/C blends with $\chi_{AB} = 20$, $\chi_{AC} = \chi_{BC} = \chi_{AD} = \chi_{CD} = 5$, $\chi_{BD} = 25$, $f_A = 0.5$, $\kappa = 0.5$, $\kappa' = 1$ and $\xi_D = 2$. Solid, dashed and dotted lines represent strong, intermediate and weak hydrogen bonding (ϵ).	51

5.11	Graphical representation of the solutions to equation (5.30) for the AB/C blends with $\chi_{AB} = 20$, $\chi_{AC} = \chi_{BC} = \chi_{AD} = \chi_{CD} = 5$, $\chi_{BD} = 25$, $f_A = 0.5$, $\kappa = 0.5$, and $\xi_D = 2$, where ϵ is fixed and the number of hydrogen-bonding sites controlled by κ' is varied.	52
5.12	RPA phase diagram for the $AB/B'D$ system with $\chi_{AB} = 15$, $\chi_{AD} = 5$ and $\chi_{BD} = 17$ with $f_A = f_D = 0.5$	53
5.13	Phase diagram for the $AB/B'D$ system with $\chi_{AB} = 15$, $\chi_{DB} = 17$ and $\chi_{AD} = 5$. Both chains are symmetrical and of equal length. Here the subscript H in ϕ_H means the hydrogen-bonded chains.	54
5.14	Normalized lamellar spacing for the $AB/B'D$ system with $\chi_{AB} = 15$, $\chi_{DB} = 17$, $\chi_{AD} = 5$ and $\xi_D=2$	55
5.15	Normalized lamellar spacing for the $AB/A'B$ system with $\chi_{AB} = 13$ and $\xi_{A'}=1.25$	56
5.16	Normalized segment length for the $AB/A'B'$ system, where λ represents the length of each segment, normalized to its initial value. . . .	57
5.17	A schematic diagram showing the increase in the lamellar spacing with increase in the $A'B'$ concentration. a) Shows a pure AB blend, b) a blend with mixed $AB/A'B'$ and c) a pure $A'B'$ blend. Increase in the $A'B'$ concentration results in a decrease in the overall lamellar spacing. . . .	58

5.18 A schematic diagram showing the shrinking of the B' chain towards the interface. a) The volume occupied by each segment is equal before the complexation. b) The volume occupied by the A' segment increases, thus increasing the interface area. To conserve the volume, the B' segment coils towards the $A'B'$ interface. The interface between the volume occupied by the $A - B$ and $A' - B'$ is assumed to be circular for simplicity. The height of each cylinder is represented by λ_α 60

Chapter 1

Introduction

The complex and elegant nature of diblock block copolymer/ homopolymer blends has attracted much attention both theoretically and experimentally over the recent years.¹⁻⁶ One of the most important properties of such blends is their ability to self-assemble into ordered structures. The size and shape of these structures can be controlled by adjusting the chemical and physical properties of the polymer chains. Some potential applications of these nano-structures include nano-lithography, photonics, data storage and drug delivery.^{1,7} Scientists and engineers often search for methods to diversify and enhance the properties of polymeric materials. One method for enriching the functionality of polymeric materials is by blending polymers of different chemical structures and architecture. Although polymer blending is a promising route, most polymer chains are immiscible due to their high degree of polymerization. The entropic term in this case is vanishingly small and the miscibility depends solely on the enthalpic term. This fact means that polymer blending often results in

macrophase separation.⁸ To induce the formation of a homogenous phase, favorable intermolecular interactions such as ion-dipole, π - π interactions or hydrogen-bonding are often utilized.^{1,8}

In this thesis, we focus on the utilization of hydrogen-bonding to enhance miscibility in AB/C blends, where hydrogen-bonds are formed between the A and C monomers. The effect of hydrogen-bonding on the phase behavior of diblock copolymer/homopolymer blends has been investigated recently in a number of experiments⁹⁻¹⁴. In particular, Chen et al.¹⁰ examined the effect of hydrogen-bonding strength on the phase transitions in AB/C systems. In this study, the authors showed that the phase behavior of the blend is affected by the strength of hydrogen-bonds formed between the A and C monomers. They observed that increasing the homopolymer concentration results in an order-order phase transition for strong hydrogen-bonding and macroscopic phase separation for weak hydrogen-bonding. In similar studies, Dobrosielska et al.^{12,14} reported on the formation of micro and macrophase separated regions in hydrogen-bonded AB/C blends. They further investigated the effect of homopolymer molecular weight on the formation of nanophase separated structures.¹² Lee et al.¹³ studied the effect of homopolymer concentration on the phase behavior of AB/C blends, where hydrogen-bonding occurs between A/C and B/C monomers. It was demonstrated that the stronger hydrogen-bonding between the A/C monomers results in a phase separated state, with the formation of mixed A/C domains in the B rich matrix.¹³ These experiments clearly indicate the importance of understanding the effect of hydrogen-bonding on polymer blending.

Although experiments provide a solid foundation for investigating hydrogen-bonding in AB/C blends, it is useful and essential to develop theoretical models for exploring the large parameter space of these complex systems. A commonly used model mimicking hydrogen-bonding between polymers assumes a large attractive (negative) interaction parameter ($\chi < 0$) between the monomers.^{13,15} Here χ is the Flory-Huggins interaction parameter. The attractive interaction provides a simple way to model the enhanced miscibility created by hydrogen-bonds. This model has been used extensively in the literature to investigate the phase behavior of hydrogen-bonded polymer blends. Han et al.¹⁵ studied the qualitative phase behavior of binary blends of block copolymers using a negative interaction parameter for modeling the formation of hydrogen-bonds between C and B monomers in AB/AC blends. Using Self-Consistent Mean Field Theory (SCFT), they investigated the phase transition sequence with respect to the AB molecular weight and volume fraction. They have reported on a qualitative agreement between the phase behavior calculated using the negative interaction SCFT model and experiments. A similar approach has been used to study hydrogen-bonding in diblock copolymer/ homopolymer blends.^{3,9,16} Lowenhaupt et al.¹⁶ studied the phase behavior of AB/A and AB/C blends using the Random-Phase Approximation (RPA) technique. They modeled the attractive interaction between the A and C monomers using a negative interaction parameter, and reported on a micro-to-macro phase transition upon increase in the C homopolymer concentration. On the other hand, it must be emphasized that, although the attractive interaction model provides a convenient method for investigating the effect of hydrogen-bonding on the phase behavior of polymer blends, it does not provide an accurate description of the hydrogen-bonding.

The correct approach for modeling hydrogen-bonding is to use interpolymer complexation, where hydrogen-bonds act as chemical bonds between the polymers, resulting in supramolecular structures. This approach has been used recently to investigate hydrogen-bonding in homopolymer/ homopolymer¹⁷⁻¹⁹ and diblock copolymer/ homopolymer blends⁵. Feng et al.¹⁹ developed a field-theoretic model for studying diblock copolymer complexes. In their work, they investigated the properties of supramolecular diblock chains formed via reversible bonding of two chemically distinct homopolymer chains¹⁹. Similar work by Nakamura and Shi examined the formation of ladder like structures formed by complete and symmetric polymer-polymer complexation.¹⁷ These studies suggest that hydrogen-bonding should be modeled by assuming a donor-acceptor relationship between monomers with hydrogen-bonding capability. Although the interpolymer complexation method provides a more accurate model of hydrogen-bonding, a comprehensive comparison between this model, the attractive interaction model and experiments has been lacking.

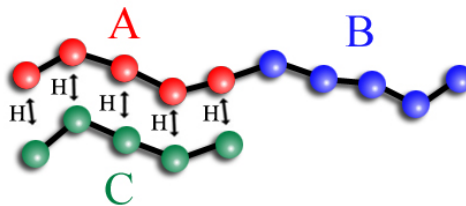


Figure 1.1: Schematic diagram for AB/C system, where the C homopolymer is capable of hydrogen bonding with block A of the diblock copolymer.

In this thesis, a detailed comparison between the attractive interaction and interpolymer complexation models is carried out for modeling hydrogen bonding in an AB/C blend. The hydrogen-bonds are assumed to occur between the A and C monomers, as shown schematically in Figure [1]. The equilibrium phase behavior of the system is calculated using SCFT. In the attractive interaction model, hydrogen-bonding is represented by assuming a large negative χ_{AC} . The strength of hydrogen-bonds is modeled by the relative magnitude of χ_{AC} . In the interpolymer complexation model, hydrogen-bonding is described as a complete and symmetric complexation between the A and C segments, where the strength of the hydrogen-bonding is represented by the number of bonds (N_D) and the energy gain per bond (ϵ). By investigating the phase behavior and lamellar spacing, it can be shown that interpolymer complexation model provides a more complete method for modeling the hydrogen-bonding between polymers.

Chapter 2

Self-Consistent Field Theory

2.1 Theoretical Framework

Developing a theoretical framework for understanding the statistical properties of block copolymers is not a trivial task. A particle-based view of polymeric melts/solutions, even those with simple chemical structures, requires a large set of variables specifying the position and velocity of every particle. This atomistic perspective is often used for small systems (approximately 1000 atoms), where the numerical solutions are computationally less expensive. An alternative method for investigating the thermodynamics of polymeric systems is the field theoretic construction of the particle based models.²⁰ In this approach a particle to field transformation is carried out.

In this thesis, the focus is on the complexation of diblock copolymers and homopolymers, resulting in the formation of complexed supramolecular structures. This process is denoted as $AB+C \rightleftharpoons A'B'C'D$, and is shown in Figure [2.1]. The prime symbol on each letter is used for bookkeeping purposes to distinguish between the A , B

and C segments in the diblock copolymer, homopolymer and complexed chains. The D segments are created by the complexation of the A and C monomers. The model

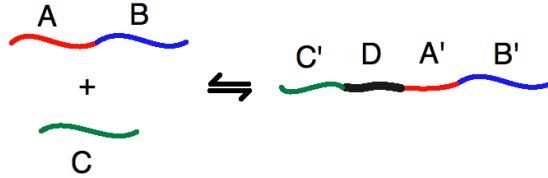


Figure 2.1: Schematic diagram showing the complexation process. The prime symbols are used for bookkeeping purposes to distinguish between the A , B and C segments in the diblock copolymer, homopolymer and complexed chains.

developed in this section considers linear complexation, where nonlinear polymer architectures are omitted for simplicity. In other words, the formation of star and/or comb like structures is not considered. To develop a theoretical framework for the interpolymer complexation model, two ingredients are required:²⁰

1. A coarse-grained model describing the conformation of polymer chains.
2. An interaction model describing the strength and type of interactions.

Conformation of the polymer chains is described by the Gaussian model²⁰, where polymer chains are considered as a sequence of spherical beads connected by freely-rotating linear springs. In this model, chains are considered flexible with a stretching

energy given by;²⁰

$$H_0[\mathbf{R}_i^\alpha(s)] = \frac{3}{2b_\alpha^2} \int_0^{N_\alpha} ds \left(\frac{d\mathbf{R}_i^\alpha(s)}{ds} \right)^2 \quad (2.1)$$

where N_α ($\alpha = A, B, C, A', B', C', D$) denotes the degrees of polymerization of the different species. The space curve $\mathbf{R}_i^\alpha(s)$ specifies the position of a given segment s , with i running over the number chains for given species. The Kuhn length b_α is used to measure the rigidity of the polymer chain. The derivative of the space curve $\mathbf{R}_i^\alpha(s)$ measures the local stretching of the chain, and thus Eq.(2.1) describes the harmonic energy associated with a given chain.

The type and strength of the interactions between segments is controlled by the Flory-Huggins parameters. The interaction between segments of two different species is represented by $\chi_{\alpha\beta}$, where $\alpha, \beta = A, B, C, A', B', C', D$. Using this notation, the interaction energy of the system is given by,

$$W[\hat{\phi}(\mathbf{r})] = \frac{\rho_o}{2} \sum_{\alpha \neq \beta} \int d\mathbf{r} \hat{\phi}_\alpha(\mathbf{r}) \hat{\phi}_\beta(\mathbf{r}) \chi_{\alpha\beta} \quad (2.2)$$

where $\hat{\phi}_\alpha(\mathbf{r})$ is the volume fraction of the α segment and ρ_o is the monomer density defined as the number monomers per unit volume. The hat ($\hat{}$) symbol on the volume fraction indicates that $\hat{\phi}(\mathbf{r})$ is a function of the chain configuration. In other words, to determine the volume fraction, one needs the information on the configuration of every chain in the system. The volume fraction ($\hat{\phi}_\alpha(\mathbf{r})$) can be written in terms of the segment density $\hat{n}_\alpha(\mathbf{r})$ at position \mathbf{r} , which is defined as,

$$\hat{n}_\alpha(\mathbf{r}) = \sum_{i=1}^{n_p} \int_0^{N_\alpha} ds \delta(\mathbf{r} - \mathbf{R}_i^\alpha(s)) \quad (2.3)$$

where n_p , with $p = 1, 2, 3$, correspond to the total number of diblock copolymer, homopolymer and complexed chains respectively. The summation in the above equation is over the total number polymers. The reference segment density ρ_o in Eq.(2.2) is $1/v_o$, with v_o being the volume occupied by a monomer. The volume fraction $\hat{\phi}_\alpha(\mathbf{r})$ in terms of $\hat{n}_\alpha(\mathbf{r})$ and v_o is written as,

$$\hat{\phi}_\alpha(\mathbf{r}) = \frac{\xi_\alpha}{\rho_o} \hat{n}_\alpha(\mathbf{r}) = \frac{\xi_\alpha}{\rho_o} \sum_{i=1}^{n_p} \int_0^{N_\alpha} ds \delta(\mathbf{r} - \mathbf{R}_i^\alpha(s)) \quad (2.4)$$

where ξ_α is the ratio between the volume of α segments and that of the reference. Using the volume fraction given by Eq.(2.4), the interaction energy for the system can be written as,

$$W[\hat{\phi}(\mathbf{r})] = \frac{1}{2} \sum_{\alpha \neq \beta} \frac{\rho_o \chi_{\alpha\beta}}{\xi_\alpha \xi_\beta} \int d\mathbf{r} \hat{\phi}_\alpha(\mathbf{r}) \hat{\phi}_\beta(\mathbf{r}) \quad (2.5)$$

The combination of Eqs.(2.1) and (2.5) defines the total energy of the system.

The statistical mechanics of our model is developed in the grand canonical ensemble with a fixed activity, volume and temperature. In this model, the activity is defined as, $z \equiv \exp[\mu_p/kT]$, with μ_p is the chemical potential of the p type chain. The number of complexed polymer chains (n_3) is dependent on the complexation between the A and C segments and therefore the maximum value which n_3 can take is equal to the minimum value of the set $\{n_1, n_2\}$. Using the notation described above, the

grand canonical partition function of the system can be written as,

$$\begin{aligned} \Xi = & \sum_{n_1=0}^{\infty} \sum_{n_2=0}^{\infty} \sum_{n_3=0}^{\text{Min}[n_1, n_2]} \frac{\lambda_1^{n_1}}{(n_1 - n_3)!} \frac{\lambda_2^{n_2}}{(n_2 - n_3)!} \frac{\lambda_3^{n_3}}{n_3!} \int D[\mathbf{R}(s)] P_0[\mathbf{R}(s)] \\ & \times \prod_{\mathbf{r}} \delta\left(\sum_{\alpha} \hat{\phi}_{\alpha}(\mathbf{r}) - 1\right) \exp\left[-W[\hat{\phi}(\mathbf{r})]\right] \end{aligned} \quad (2.6)$$

where λ_1 , λ_2 and λ_3 are the fugacity of the diblock copolymer, homopolymer and complexed polymer chains, respectively. The incompressibility of the segments is imposed by the delta function in Eq.(2.6). This condition ensures that at every point in space, the volume fraction of all species must add up to one. The stretching energy of the chains defined by Eq.(2.1), is captured by $P_0[\mathbf{R}(s)]$, which can be written as,

$$\begin{aligned} P_0[\mathbf{R}(s)] = & \left[\prod_{\alpha=A, B} \prod_{i=1}^{n_1 - n_3} P_0(\mathbf{R}_i^{\alpha}(s)) \delta[\mathbf{R}_i^A(N_A) - \mathbf{R}_i^B(N_B)] \right] \left[\prod_{j=1}^{n_2 - n_3} P_0(\mathbf{R}_j^C(s)) \right] \\ & \left[\prod_{\beta=A', B', C', D} \prod_{l=1}^{n_3} P_0(\mathbf{R}_l^{\beta}(s)) \delta[\mathbf{R}_l^{A'}(N_{A'}) - \mathbf{R}_l^{B'}(N_{B'})] \delta[\mathbf{R}_l^{A'}(0) - \mathbf{R}_l^D(N_D)] \right. \\ & \left. \delta[\mathbf{R}_l^{C'}(N_{C'}) - \mathbf{R}_l^D(0)] \right] \end{aligned} \quad (2.7)$$

where the delta functions ensure the connectivity of the chains. For example the end segments N_A and N_B are connected to create the diblock copolymer AB . The probabilities $P_0(\mathbf{R}_i^{\alpha}(s))$ in Eq.(2.7) are known as the Wiener measure and have the form,

$$P_0(\mathbf{R}_i^{\alpha}(s)) = \tilde{A} \exp\left[\frac{-3}{2b_{\alpha}^2} \int_0^{N_{\alpha}} ds \left(\frac{d\mathbf{R}_i^{\alpha}(s)}{ds}\right)^2\right] \quad (2.8)$$

where \tilde{A} is a normalization constant. The expression inside the exponential in the above equation is the chain stretching Hamiltonian defined in Eq.(2.1). Equation

(2.8) describes the chain configuration probability.

Analytical evaluation of the partition function (2.6) is not possible, because it depends on the chain conformation through the volume fraction elements. A common mathematical trick for solving the partition function is by introducing a dummy function $\phi(\mathbf{r})$, which couples to the volume fraction $\hat{\phi}(\mathbf{r})$. This can be written mathematically as,

$$1 = \int D[\phi_\alpha] \prod_\alpha \prod_{\mathbf{r}} \frac{\rho_o}{\xi_\alpha} \delta(\phi_\alpha(\mathbf{r}) - \hat{\phi}_\alpha(\mathbf{r})) \quad (2.9)$$

By inserting this identity into Eq.(2.6), the conformation dependence of the partition function (2.6) can be separated from the interaction term.

$$\begin{aligned} \Xi &= \sum_{n_1=0}^{\infty} \sum_{n_2=0}^{\infty} \sum_{n_3=0}^{\text{Min}[n_1, n_2]} \frac{\lambda_1^{n_1}}{(n_1 - n_3)!} \frac{\lambda_2^{n_2}}{(n_2 - n_3)!} \frac{\lambda_3^{n_3}}{n_3!} \int D[\mathbf{R}(s)] P_0[\mathbf{R}(s)] D[\phi_\alpha] \\ &\times \prod_\alpha \prod_{\mathbf{r}} \delta\left(\sum_\alpha \phi_\alpha(\mathbf{r}) - 1\right) \frac{\rho_o}{\xi_\alpha} \delta(\phi_\alpha(\mathbf{r}) - \hat{\phi}_\alpha(\mathbf{r})) \exp[-W[\phi(\mathbf{r})]] \quad (2.10) \end{aligned}$$

Using the Fourier transform representation of the identity (2.9), the partition function (2.10) is further modified. This transformation introduces auxiliary fields $\omega_\alpha(\mathbf{r})$, which couple to the volume fractions $\phi_\alpha(\mathbf{r})$.

$$\begin{aligned} \Xi &= \sum_{n_1=0}^{\infty} \sum_{n_2=0}^{\infty} \sum_{n_3=0}^{\text{Min}[n_1, n_2]} \frac{\lambda_1^{n_1}}{(n_1 - n_3)!} \frac{\lambda_2^{n_2}}{(n_2 - n_3)!} \frac{\lambda_3^{n_3}}{n_3!} \int D[\phi(\mathbf{r})] D[\omega(\mathbf{r})] \prod_{\mathbf{r}} \delta\left(\sum_\alpha \phi_\alpha(\mathbf{r}) - 1\right) \\ &\times \exp\left[\sum_\alpha \int d\mathbf{r} \frac{\rho_o \omega_\alpha(\mathbf{r}) \phi_\alpha(\mathbf{r})}{\xi_\alpha} - W[\phi(\mathbf{r})]\right] \int D[\mathbf{R}(s)] P_0[\mathbf{R}(s)] \\ &\times \exp\left[-\sum_\alpha \int d\mathbf{r} \frac{\rho_o \omega_\alpha(\mathbf{r}) \hat{\phi}_\alpha(\mathbf{r})}{\xi_\alpha}\right] \quad (2.11) \end{aligned}$$

The above mathematical treatment has transformed the many body interaction into

the interaction of a single chain with fields $\phi_\alpha(\mathbf{r})$ and $\omega_\alpha(\mathbf{r})$. The conformation dependence of the partition function is now captured by the single chain partition function. Using Eqs.(2.7), (2.8) and (2.11), the single chain partition functions for the diblock copolymer, homopolymer and complexed chains can be written as,

$$Q_1 = \frac{1}{V} \int D[\mathbf{R}^A(s)]D[\mathbf{R}^B(s)]P_0[\mathbf{R}^A(s)]P_0[\mathbf{R}^B(s)]\exp\left[-\sum_{\alpha=A,B} \int_0^{N_\alpha} ds \omega_\alpha[\mathbf{R}^\alpha(s)]\right] \times \delta(\mathbf{R}^A(N_A) - \mathbf{R}^B(N_B)) \quad (2.12)$$

$$Q_2 = \frac{1}{V} \int D[\mathbf{R}^C(s)]P_0[\mathbf{R}^C(s)]\exp\left[-\int_0^{N_C} ds \omega_C[\mathbf{R}^C(s)]\right] \quad (2.13)$$

$$Q_3 = \frac{1}{V} \int D[\mathbf{R}^{A'}(s)]D[\mathbf{R}^{B'}(s)]D[\mathbf{R}^{C'}(s)]D[\mathbf{R}^D(s)]P_0[\mathbf{R}^{A'}(s)]P_0[\mathbf{R}^{B'}(s)]P_0[\mathbf{R}^{C'}(s)] \times P_0[\mathbf{R}^D(s)] \exp\left[-\sum_{\alpha=A',B',C',D} \int_0^{N_\alpha} ds \omega_\alpha[\mathbf{R}^\alpha(s)]\right] \delta[\mathbf{R}^{A'}(N_{A'}) - \mathbf{R}^{B'}(N_{B'})] \times \delta[\mathbf{R}^{A'}(0) - \mathbf{R}^D(N_D)]\delta[\mathbf{R}^D(0) - \mathbf{R}^{C'}(N_{C'})] \quad (2.14)$$

where V is the total volume of the system. Using the above definition, the grand canonical partition function is written as,

$$\Xi = \sum_{n_1=0}^{\infty} \sum_{n_2=0}^{\infty} \sum_{n_3=0}^{\text{Min}[n_1, n_2]} \frac{\lambda_1^{n_1}}{(n_1 - n_3)!} \frac{\lambda_2^{n_2}}{(n_2 - n_3)!} \frac{\lambda_3^{n_3}}{n_3!} [Q_1 V]^{n_1 - n_3} [Q_2 V]^{n_2 - n_3} [Q_3 V]^{n_3} \times \int D[\phi(\mathbf{r})]D[\omega(\mathbf{r})] \prod_{\mathbf{r}} \delta\left(\sum_{\alpha} \phi_\alpha(\mathbf{r}) - 1\right) \exp\left[\sum_{\alpha} \int d\mathbf{r} \frac{\rho_o \omega_\alpha(\mathbf{r}) \phi_\alpha(\mathbf{r})}{\xi_\alpha} - W[\phi(\mathbf{r})]\right] \quad (2.15)$$

By applying the following transformation,

$$\sum_{n_1=0}^{\infty} \sum_{n_2=0}^{\infty} \sum_{n_3=0}^{\text{Min}[n_1, n_2]} \longrightarrow \sum_{\sigma_1=0}^{\infty} \sum_{\sigma_2=0}^{\infty} \sum_{\sigma_3=0}^{\infty}$$

$$\frac{(\lambda_1)^{n_1}}{(n_1 - n_3)!} \frac{(\lambda_2)^{n_2}}{(n_2 - n_3)!} \frac{(\lambda_3)^{n_3}}{n_D!} \longrightarrow \frac{(\lambda_1)^{(\sigma_1 + \sigma_3)}}{\sigma_1!} \frac{(\lambda_2)^{(\sigma_2 + \sigma_3)}}{\sigma_2!} \frac{(\lambda_3)^{\sigma_3}}{\sigma_3!} \quad (2.16)$$

the partition function can be written as,

$$\Xi = \int D[\phi(\mathbf{r})] D[\omega(\mathbf{r})] \prod_{\mathbf{r}} \delta\left(\sum_{\alpha} \phi_{\alpha}(\mathbf{r}) - 1\right) \exp\left[\sum_{\alpha} \int d\mathbf{r} \frac{\rho_o \omega_{\alpha}(\mathbf{r}) \phi_{\alpha}(\mathbf{r})}{\xi_{\alpha}} - W[\phi(\mathbf{r})] + \lambda_1 Q_1 V + \lambda_2 Q_2 V + \lambda_1 \lambda_2 \lambda_3 Q_3 V\right] \quad (2.17)$$

The Fourier representation of the incompressibility condition is used to further simplify the partition function. This modification, introduces an extra field ($\eta(\mathbf{r})$) to ensure the incompressibility in the system. This extra field is a Lagrangian multiplier²¹, and the grand canonical partition function in terms of $\phi(\mathbf{r})$, $\omega(\mathbf{r})$ and $\eta(\mathbf{r})$ fields becomes

$$\Xi = \int D[\phi(\mathbf{r})] D[\omega(\mathbf{r})] D[\eta(\mathbf{r})] \exp\left[-\int d\mathbf{r} \eta(\mathbf{r}) \left(\sum_{\alpha} \phi_{\alpha}(\mathbf{r}) - 1\right) + \sum_{\alpha} \int d\mathbf{r} \frac{\rho_o \omega_{\alpha}(\mathbf{r}) \phi_{\alpha}(\mathbf{r})}{\xi_{\alpha}} - W[\phi(\mathbf{r})] + \lambda_1 Q_1 V + \lambda_2 Q_2 V + \lambda_1 \lambda_2 \lambda_3 Q_3 V\right] \quad (2.18)$$

The above grand canonical partition function is written in terms of a free energy functional $G(\phi, \omega, \eta)$, $\Xi = \int D[\phi] D[\omega] \exp[-G(\phi, \omega, \eta)]$, where the free energy $G(\phi, \omega, \eta)$

is given by,

$$G(\phi, \omega, \eta) = \int d\mathbf{r} \eta(\mathbf{r}) \left(\sum_{\alpha} \phi_{\alpha}(\mathbf{r}) - 1 \right) - \sum_{\alpha} \int d\mathbf{r} \frac{\rho_{\alpha} \omega_{\alpha}(\mathbf{r}) \phi_{\alpha}(\mathbf{r})}{\xi_{\alpha}} + W[\phi(\mathbf{r})] - \lambda_1 Q_1 V - \lambda_2 Q_2 V - \lambda_1 \lambda_2 \lambda_3 Q_3 V \quad (2.19)$$

Although the above form of the partition function seems simple, it is not possible to evaluate its solutions in closed form.

One of the most popular techniques for evaluating the above partition function is the mean-field approximation, or the SCFT²⁰. The basic idea of SCFT is that the functional integral (2.18) in equilibrium is dominated by a set of specific field configurations $\tilde{\phi}(\mathbf{r})$, $\tilde{\omega}(\mathbf{r})$ and $\tilde{\eta}(\mathbf{r})$, where these configurations are the stationary points of the free energy functional $G(\phi, \omega, \eta)$. This requires evaluating

$$\frac{\delta G(\phi, \omega, \eta)}{\delta \phi} = \frac{\delta G(\phi, \omega, \eta)}{\delta \omega} = \frac{\delta G(\phi, \omega, \eta)}{\delta \eta} = 0 \quad (2.20)$$

which results in the Self-Consistent Field Equations (SCFE). Taking the degree of polymerization of the diblock chain (N_1) as the reference, the relative size of the homopolymer and the complex chains can be written as

$$\begin{aligned} \kappa &= \frac{N_2}{N_1} \\ \kappa' &= \frac{N_3}{N_1} \end{aligned} \quad (2.21)$$

Using κ and κ' and the condition $f_A + f_B = 1$, the segment fractions of the complexed

chain become,

$$\begin{aligned}
f_{A'} &= \frac{f}{\kappa'} - \frac{1 + \kappa}{\kappa'} + 1 \\
f_{B'} &= \frac{(1 - f)}{\kappa'} \\
f_{C'} &= 1 - \frac{1}{\kappa'} \\
f_D &= \frac{1 + \kappa}{\kappa'} - 1
\end{aligned} \tag{2.22}$$

where $f_{A'} + f_{B'} + f_{C'} + f_D = 1$. Using the above notation, carrying out the functional derivatives of Eq.(2.19) results in,

$$\begin{aligned}
\frac{\phi_\alpha(\mathbf{r})}{\xi_\alpha} &= \lambda_1 \lambda_{01} \int_0^{f_\alpha} ds q_\alpha(\mathbf{r}, s) q_\alpha^\dagger(\mathbf{r}, f_\alpha - s) \\
\frac{\phi_C(\mathbf{r})}{\xi_C} &= \frac{\lambda_2 \lambda_{02}}{\kappa} \int_0^\kappa ds q_C(\mathbf{r}, s) q_C(\mathbf{r}, \kappa - s) \\
\frac{\phi_\beta(\mathbf{r})}{\xi_\beta} &= \frac{\lambda_1 \lambda_2 \lambda_3 \lambda_{03}}{\kappa'} \int_0^{\kappa' f_\beta} ds q_\beta(\mathbf{r}, s) q_\beta^\dagger(\mathbf{r}, \kappa' f_\beta - s) \\
\frac{\omega_\gamma(\mathbf{r})}{\xi_\gamma} &= \frac{1}{2} \sum_{\gamma \neq \gamma'} \frac{\phi_{\gamma'}(\mathbf{r}) \chi_{\gamma\gamma'}}{\xi_\gamma \xi_{\gamma'}} + \eta(\mathbf{r}) \\
\sum_\gamma \phi_\gamma(\mathbf{r}) &= 1
\end{aligned} \tag{2.23}$$

where $(\alpha = A, B)$, $(\beta = A', B', C', D)$ and $(\gamma, \gamma' = A, B, C, A', B', C', D)$. In the above set of equations, q and q^\dagger are the forward and complementary end-integrated propagators. The chain propagators are defined as,

$$Q_\alpha(\mathbf{r}, s | \mathbf{r}', 0) = \int_{\mathbf{R}(0)=\mathbf{r}'}^{\mathbf{R}(s)=\mathbf{r}} D[\mathbf{R}(s)] \exp \left[- \int_0^{N_\alpha} ds \left(\frac{3}{2b_\alpha^2} \left(\frac{d\mathbf{R}(s)}{ds} \right)^2 + \omega_\alpha(\mathbf{R}(s)) \right) \right] \tag{2.24}$$

where $Q_\alpha(\mathbf{r}, s | \mathbf{r}', 0)$ corresponds to the conditional probability of segment s being

found at position \mathbf{r} , given that segment 0 was at position \mathbf{r}' . The propagator given in Eq.(2.24) is closely related to the quantum propagator constructed using the Feynman path integrals²². The end-integrated propagators are calculated as,

$$\begin{aligned} q_\alpha(\mathbf{r}, s) &= \int d\mathbf{r}' Q_\alpha(\mathbf{r}, s | \mathbf{r}', 0) \\ q_\alpha^\dagger(\mathbf{r}, s) &= \int d\mathbf{r}' d\mathbf{r}'' Q_\alpha(\mathbf{r}, s | \mathbf{r}', 0) Q_\beta(\mathbf{r}', N_\beta | \mathbf{r}'', 0) \end{aligned} \quad (2.25)$$

Figure[2.2] is a diagram showing the end-integrated propagators for a given segment s . The $q(\mathbf{r}, s)$ function describes the conditional probability of going from one end of the chain to the segment s . Similarly, $q^\dagger(\mathbf{r}, f - s)$ defines the conditional probability of going from the other end of the chain to the joining segment and then to segment s . By discretizing the chain and using Taylor expansion,²⁰ it can be shown that the

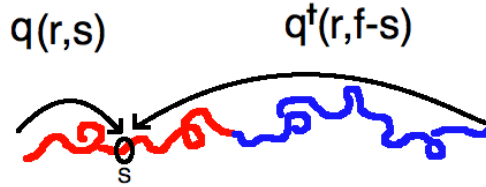


Figure 2.2: Schematic diagram showing the end integrated propagators for a diblock chain.

propagators satisfy a Fokker-Planck like equation known as the modified diffusion equation^{20,21}. These equations for the forward and complementary end-integrated

propagators are

$$\begin{aligned}\frac{\partial q_\alpha(\mathbf{r}, s)}{\partial s} &= \frac{N_1 b_\alpha^2}{6} \nabla^2 q_\alpha(\mathbf{r}, s) - N_1 \omega_\alpha(\mathbf{r}) q_\alpha(\mathbf{r}, s) \\ -\frac{\partial q_\alpha^\dagger(\mathbf{r}, s)}{\partial s} &= \frac{N_1 b_\alpha^2}{6} \nabla^2 q_\alpha^\dagger(\mathbf{r}, s) - N_1 \omega_\alpha(\mathbf{r}) q_\alpha^\dagger(\mathbf{r}, s)\end{aligned}\quad (2.26)$$

where s runs from 0 to N_α . Equations (2.26) describe the diffusion of a particle through fields ω_α , with the time variable being replaced by the segment number. The length scale in the system can be scaled by R_g^2 , where R_g^2 defines the average size of a polymer chain. This quantity is the root-mean-squared distance between the segments and the center of the mass. Given the appropriate initial and boundary conditions, the above modified diffusion equations can be solved. The numerical treatment of the modified diffusion equation is described extensively in chapter four.

Solving equations (2.26) requires the initial configuration of the $\omega_\alpha(\mathbf{r})$ fields. This initial configuration often depends on the numerical technique and the specifics of the model. Assuming that the initial $\omega_\alpha(\mathbf{r})$ fields are given, $q(\mathbf{r}, s)$ and $q^\dagger(\mathbf{r}, s)$ can be calculated. With this information, the SCFE and the free energy of the system can be evaluated. If the initial $\omega(\mathbf{r})$ and the calculated $\phi(\mathbf{r})$ and $\eta(\mathbf{r})$ fields are the saddle point solutions to the mean field approximation, then the iteration process is done. Otherwise, new $\omega(\mathbf{r})$ fields can be constructed by a small perturbation about the original fields. This process is iterated until the self-consistent solutions are achieved.

2.2 The Homogenous Phase

The self-consistent field equations (2.23) are the saddle-point solutions of the free energy functional $G(\phi, \omega, \eta)$. The simplest solution of the SCFE is that of the homogenous phase, where the ϕ , ω and η fields are uniform. The single chain partition functions given by Eqs.(2.12), (2.13) and (2.14) in the homogenous phase can be written as

$$\begin{aligned}
 Q_1 &= \exp\left[-\omega_A f_A - \omega_B f_B\right] \\
 Q_2 &= \exp\left[-\kappa \omega_C\right] \\
 Q_3 &= \exp\left[\kappa' (-\omega_{A'} f_{A'} - \omega_{B'} f_{B'} - \omega_{C'} f_{C'} - \omega_D f_D)\right]
 \end{aligned} \tag{2.27}$$

where the stretching energy is set to zero. Similarly, the self-consistent field equations can be written as

$$\begin{aligned}
 \bar{\phi}_1 &= \lambda_1 \lambda_{01} Q_1 \\
 \bar{\phi}_2 &= \lambda_2 \lambda_{02} Q_2 \\
 \bar{\phi}_3 &= \lambda_1 \lambda_2 \lambda_3 \lambda_{03} \Psi Q_3 \\
 \frac{\bar{\omega}_\alpha}{\xi_\alpha} &= \sum_{\beta \neq \alpha} \frac{\bar{\phi}_\beta \chi_{\alpha\beta}}{\xi_\alpha \xi_\beta} + \eta \\
 \sum_\alpha \bar{\phi}_\alpha &= 1
 \end{aligned} \tag{2.28}$$

where $\Psi = f_{A'} + f_{B'} + f_{C'} + \xi_D f_D$. In the above set of equations, the monomer size of the single-stranded chains is used as the reference. This means that $\xi_\alpha = 1$ for $\alpha = A, B, C, A', B'$ and C' . The free energy functional $G(\phi, \omega, \eta)$ for the homogenous

phase becomes,

$$G_H(\phi, \omega, \eta) = \sum_{\alpha} \frac{\bar{\omega}_{\alpha} \bar{\phi}_{\alpha}}{\bar{\xi}_{\alpha}} - \frac{1}{2} \sum_{\alpha \neq \beta} \frac{\chi_{\alpha\beta} \bar{\phi}_{\alpha} \bar{\phi}_{\beta}}{\bar{\xi}_{\alpha} \bar{\xi}_{\beta}} + \lambda_1 Q_1 + \frac{\lambda_2 Q_2}{\kappa} + \frac{\lambda_1 \lambda_2 \lambda_3 Q_3}{\kappa'} \quad (2.29)$$

where the bar symbol corresponds to the average value of the parameters. Using the homogenous mean field equations (2.28), the free energy (2.29) can be rewritten as,

$$G_H(\phi, \omega, \eta) = \sigma \bar{\phi}_s - \frac{\theta \bar{\phi}_s}{\kappa} - \frac{1 - \bar{\phi}_s}{\Psi \kappa'} + W(\bar{\phi}_s) + \sigma \bar{\phi}_s \ln(\sigma \bar{\phi}_s) + \frac{\theta \bar{\phi}_s}{\kappa} \ln(\theta \bar{\phi}_s) + \frac{1 - \bar{\phi}_s}{\kappa' \Psi} \ln\left(\frac{1 - \bar{\phi}_s}{\Psi}\right) - \bar{\phi}_s [\ln(\Lambda) + \ln(z)] \quad (2.30)$$

where $\bar{\phi}_s$ is the volume fraction of the single-strand chains in the homogenous phase. This parameter can be written in terms of the volume fraction of the diblock copolymer and homopolymer chains such that $\bar{\phi}_s = \sigma \bar{\phi}_1 + \theta \bar{\phi}_2$, where $\bar{\phi}_1 = \bar{\phi}_A + \bar{\phi}_B$ and $\bar{\phi}_2 = \bar{\phi}_C$. Because the incompressibility condition requires that $\bar{\phi}_1 + \bar{\phi}_2 + \bar{\phi}_3 = 1$, it is possible to write $\bar{\phi}_3$ as $1 - \bar{\phi}_s$. The parameters z and Λ in the last part of equation (2.30) contain the chemical potential contribution to the free energy. They can be defined as,

$$z = \exp\left[\mu_1\left(\sigma - \frac{1}{\Psi \kappa'}\right) + \mu_2\left(\frac{\theta}{\kappa} - \frac{1}{\Psi \kappa'}\right) - \frac{\epsilon f_D N_1}{\Psi} - \frac{\mu_3}{\kappa' \Psi}\right] \\ \Lambda = N_1^{\sigma + \frac{\theta}{\kappa} - \frac{1}{\kappa' \Psi}} \kappa^{\frac{\theta}{\kappa}} \kappa'^{\frac{-1}{\kappa' \Psi}} \quad (2.31)$$

where μ_1 , μ_2 and μ_3 are chemical potentials of diblock copolymer, homopolymer and complexed polymer chains respectively. The strength of a single hydrogen-bond

is described by the parameter ϵ . By fixing these parameters, the homogenous free energy can be calculated. This energy is the reference with respect to which the free energy of heterogeneous phases are calculated.

At the equilibrium state, the fraction of the complexed chains can be determined by applying the mass action law. The mass action law is determined by chemical equilibrium. For the specific case of AB/C system, the mass action law can be written as,

$$\frac{1 - \bar{\phi}_s}{\sigma \bar{\phi}_s \rho \bar{\phi}_s} = K_{eq} \quad (2.32)$$

where K_{eq} is the equilibrium constant. Using the self-consistent field equations (2.28), the above mass action law can be written as,

$$\frac{1 - \bar{\phi}_s}{\sigma \theta \bar{\phi}_s^2} = \frac{\kappa'}{\kappa N_1 \rho_o} \frac{Q_3}{Q_1 Q_2} \quad (2.33)$$

where the analysis of the solutions to this equation would allow for determining the fraction of the complexed chains at the equilibrium state. The solutions to equation (2.33) for various degree of polymerization and hydrogen-bonding strengths are investigated in chapter five.

Chapter 3

The Random Phase Approximation

The Self-Consistent Field Theory developed in the previous section for the complexation model is specified by a large number of parameters, resulting in a large parameter space. Investigating the phase behavior of the AB/C blend requires exploring this parameter space. This task could be computationally expensive and thus an approximate description of the phase behavior, prior to solving the SCFT, is desirable. The Random Phase Approximation technique (RPA) allows for the determination of the stability of the homogenous (or disordered) phase, thus providing an overall picture of the phase behavior of a polymeric system.²¹ Leibler^{23,24} was the first to use random phase approximation to analyze the microphase separation of diblock copolymers, particularly the order-disorder phase transition. The calculation done by Leibler can be extended to the complexation model developed in chapter two.

The stability of the disordered phase is determined by analyzing the free energy difference (ΔF) between that of the homogenous phase and the phase created by adding small fluctuations to the homogenous phase. The order parameter $\delta\phi(\mathbf{r})$ in

this model is defined as,

$$\delta\phi_\alpha(\mathbf{r}) = \phi_\alpha(\mathbf{r}) - \bar{\phi}_\alpha \quad (3.1)$$

Using this order parameter we can re-express the free energy functional in terms of $\delta\phi_\alpha(\mathbf{r})$. It is important to note that only small fluctuations about the average, created by some external fields W_α , are considered. The interaction between the segments are not considered at this point, but will be introduced later. The free energy difference ΔF can be written as

$$F[\delta\phi(\mathbf{r})] - F[0] = -\ln\left[\frac{\sum_{n=1,2,3} Q_n[W(\mathbf{r})]}{Q[0]}\right] - \sum_\alpha \int d\mathbf{r} W_\alpha(\mathbf{r}) \delta\phi_\alpha(\mathbf{r}) \quad (3.2)$$

where $F[0]$ is the free energy of the system with no density fluctuations (the free energy of the disordered phase). As before, $\alpha = A, B, C, A', B', C', D$ and $Q[W(\mathbf{r})]$ and $Q[0]$ are the single chain partition functions of diblock, homopolymer and complexed chains in the perturbed and homogenous phase, respectively. Because there are no density fluctuations in the homogenous (disordered) phase, the external fields $W_\alpha(\mathbf{r})$ are set to zero.

Since only small fluctuations about the disordered phase are considered, the right hand side of the Eq.(3.2) can be expanded in a functional Taylor series around $W_\alpha(\mathbf{r})$.

²¹ Taking the Fourier transform of this expansion and keeping only the first non-zero term results in,

$$F[\delta\phi_\alpha(\mathbf{q})] - F[0] = \frac{1}{2} \sum_{\alpha\beta} \sum_{\mathbf{q}} \frac{\delta\phi_\alpha(\mathbf{q})\delta\phi_\beta(\mathbf{q})}{S_{\alpha\beta}^*(\mathbf{q})} + \dots \quad (3.3)$$

In the above equation, $S_{\alpha\beta}^*(\mathbf{q})$ is the Fourier transform of the two point correlation function in the phase created by the small fluctuations. Stability of the homogenous phase is determined by analyzing the eigenvalues $\lambda_i(\mathbf{q})$ of the correlation matrix. The entries of this matrix are the two point correlation functions $S_{\alpha\beta}^*(\mathbf{q})$.

By considering the condition that small density fluctuations $\delta\phi_\alpha(\mathbf{r})$ are coupled to weak artificial external fields $W_\alpha(\mathbf{r})$, the following linear relation can be written,

$$\frac{\delta\phi_\alpha(\mathbf{q})}{\xi_\alpha} = - \sum_{\beta} S_{\alpha\beta}^0(\mathbf{q}) W_\beta(\mathbf{q}) \quad (3.4)$$

In the above equation, $S_{\alpha\beta}^0(\mathbf{q})$ are the two-point correlation functions in the homogenous phase. The $W_\beta(\mathbf{q})$ fields can be divided into two parts; $\omega_\beta^{EX}(\mathbf{q})$, which are the artificial external fields and $\omega_\beta^{RPA}(\mathbf{q})$, which contain the contribution from the interactions between the segments. The $\omega_\beta^{RPA}(\mathbf{q})$ fields for an incompressible system can be written as,

$$\frac{\omega_\beta^{RPA}(\mathbf{q})}{\xi_\beta} = \sum_{\alpha} \frac{\chi_{\beta\alpha} \delta\phi_\alpha(\mathbf{q})}{\xi_\alpha \xi_\beta} + \eta \quad (3.5)$$

where η is the Lagrange multiplier. Introducing Eq.(3.5) into (3.4) results in,

$$\frac{\delta\phi_\alpha(\mathbf{q})}{\xi_\alpha} = - \sum_{\beta} S_{\alpha\beta}^0(\mathbf{q}) \left[\omega_\beta^{EX}(\mathbf{q}) + \sum_{\gamma \neq \beta} \frac{\chi_{\beta\gamma} \delta\phi_\gamma(\mathbf{q})}{\xi_\gamma \xi_\beta} + \eta \right] \quad (3.6)$$

where the incompressibility condition (neglecting short length fluctuations) ensures that $\sum_{\alpha} \delta\phi_\alpha = 0$. Enforcing this condition, one could solve for η and insert it back

into equation (3.6) to get the response of the density function to the external fields $\omega_\alpha^{EX}(\mathbf{q})$. The spatial structure of the heterogenous phase, formed by the small density fluctuations, is characterized by $S_{\alpha\beta}^*(\mathbf{q})$.

Solving for η in the above expression is most simply done by writing Eq.(3.6) in the matrix form;

$$\begin{bmatrix} \delta\phi_1(\mathbf{q})/\xi_1 \\ \delta\phi_2(\mathbf{q})/\xi_2 \\ \cdot \\ \cdot \\ \cdot \\ \delta\phi_m(\mathbf{q})/\xi_m \end{bmatrix} = - \begin{bmatrix} S_{11}^0(\mathbf{q}) & S_{12}^0(\mathbf{q}) & \dots & S_{1m}^0(\mathbf{q}) \\ S_{21}^0(\mathbf{q}) & S_{22}^0(\mathbf{q}) & \dots & S_{2m}^0(\mathbf{q}) \\ \cdot & \cdot & \dots & \cdot \\ \cdot & \cdot & \dots & \cdot \\ \cdot & \cdot & \dots & \cdot \\ S_{m1}^0(\mathbf{q}) & S_{m2}^0(\mathbf{q}) & \dots & S_{mm}^0(\mathbf{q}) \end{bmatrix} \times \left\{ \begin{bmatrix} \omega_1^{EX}(\mathbf{q}) \\ \omega_2^{EX}(\mathbf{q}) \\ \cdot \\ \cdot \\ \cdot \\ \omega_m^{EX}(\mathbf{q}) \end{bmatrix} + \begin{bmatrix} \omega_1^{RPA}(\mathbf{q}) \\ \omega_2^{RPA}(\mathbf{q}) \\ \cdot \\ \cdot \\ \cdot \\ \omega_m^{RPA}(\mathbf{q}) \end{bmatrix} \right\}$$

where $S_{ij}^0(\mathbf{q})$ is the two-point correlation function between the i^{th} and j^{th} component.

The above matrix notation in a compact form is written as,

$$\delta\vec{\phi} = -\mathbf{S}^0[\vec{\omega}^{EX} + \vec{\omega}^{RPA}] - \mathbf{S}^0[\vec{\omega}^{EX} + \mathbf{X} \delta\vec{\phi} + \vec{\eta}] \quad (3.7)$$

where \mathbf{S}^0 and \mathbf{X} are the correlation function and interaction parameter matrices, and $\delta\vec{\phi}$, $\vec{\omega}^{EX}$ and $\vec{\eta}$ are density, external field and Lagrange multiplier arrays respectively.

Using the condition $\sum_\alpha \delta\vec{\phi}_\alpha = 0$, (3.7) is solved to give an explicit expression for η .

$$\eta = -\frac{\vec{i}^T \mathbf{A}^{-1} \mathbf{S}^0 \vec{\omega}^{EX}}{\vec{i}^T \mathbf{A}^{-1} \mathbf{S}^0 \vec{i}} \vec{i} \quad (3.8)$$

Here η is a constant and not a vector, and i and i^T are defined as,

$$\vec{i} = \begin{bmatrix} 1 \\ 1 \\ \cdot \\ \cdot \\ \cdot \\ 1 \end{bmatrix} \quad \vec{i}^T = \begin{bmatrix} 1 & 1 & \cdot & \cdot & \cdot & 1 \end{bmatrix}$$

In equation (3.8), \mathbf{A}^{-1} is an inverse of the \mathbf{A} matrix, where \mathbf{A} is defined as,

$$\mathbf{A} = [\mathbf{I} + \mathbf{S}^0 \mathbf{X}] \quad (3.9)$$

where \mathbf{I} is an $m \times m$ identity matrix. Using the expression for η in equation (3.7) and with the help of little algebra, one could write

$$\begin{aligned} \delta\vec{\phi} &= \mathbf{A}^{-1} \left[-\mathbf{S}^0 \vec{\omega}^{EX} - \mathbf{S}^0 \vec{\eta} \right] \\ &= \mathbf{A}^{-1} \left[-\mathbf{S}^0 \vec{\omega}^{EX} + \frac{\mathbf{S}^0 \tilde{\mathbf{I}} \mathbf{A}^{-1} \mathbf{S}^0 \vec{\omega}^{EX}}{\vec{i}^T \mathbf{A}^{-1} \mathbf{S}^0 \vec{i}} \right] \\ &= - \left[\mathbf{A}^{-1} \mathbf{S}^0 - \frac{\mathbf{A}^{-1} \mathbf{S}^0 \tilde{\mathbf{I}} \mathbf{A}^{-1} \mathbf{S}^0}{\vec{i}^T \mathbf{A}^{-1} \mathbf{S}^0 \vec{i}} \right] \vec{\omega}^{EX} \\ &= -\mathbf{S}^* \vec{\omega}^{EX} \end{aligned} \quad (3.10)$$

where \mathbf{S}^* is an $m \times m$ matrix and $\tilde{\mathbf{I}} = \vec{i} \cdot \vec{i}^T$. The elements of the \mathbf{S}^* matrix are the two-point correlation functions of the phase created by the small density fluctuations. The stability of the homogenous phase is determined by analyzing the eigenvalues of the \mathbf{S}^* matrix. Throughout this calculation, the structure of the polymer chains has

not been discussed. This means that the method developed here can be applied to any chain architecture. To apply the above formalism to the complexation model, one needs to specify the elements of the \mathbf{S}^0 matrix. These elements are the scattering intensities known as Debye functions.²¹ They describe the two-point correlation of an ideal chain in the absence of any external fields. These conditions describe the state of the homogenous phase.

As an example, the \mathbf{S}^0 matrix for the AB/DB' system, which results from complete complexation, is shown and discussed. The scattering intensity matrix, \mathbf{S}^0 , for the above system is a 4×4 matrix,

$$\mathbf{S}^0 = \begin{bmatrix} S_{AA}(\mathbf{q}) & S_{AB}(\mathbf{q}) & 0 & 0 \\ S_{AB}(\mathbf{q}) & S_{BB}(\mathbf{q}) & 0 & 0 \\ 0 & 0 & S_{B'B'}(\mathbf{q}) & S_{B'D}(\mathbf{q}) \\ 0 & 0 & S_{B'D}(\mathbf{q}) & S_{DD}(\mathbf{q}) \end{bmatrix}$$

The elements of this matrix are given by,

$$\begin{aligned} S_{AA}(\mathbf{q}) &= \frac{2\phi}{\mathbf{q}^2} \left[e^{-f_A \mathbf{q}} + f_A \mathbf{q} - 1 \right] \\ S_{AB}(\mathbf{q}) &= \frac{\phi}{\mathbf{q}^2} \left[(1 - e^{-f_A \mathbf{q}})(1 - e^{-f_B \mathbf{q}}) \right] \\ S_{BB}(\mathbf{q}) &= \frac{2\phi}{\mathbf{q}^2} \left[e^{-f_B \mathbf{q}} + f_B \mathbf{q} - 1 \right] \\ S_{B'B'}(\mathbf{q}) &= \frac{2(1 - \phi)}{\kappa \mathbf{q}^2} \left[e^{-\kappa f_{B'} \mathbf{q}} + \kappa f_{B'} \mathbf{q} - 1 \right] \\ S_{B'D}(\mathbf{q}) &= \frac{1 - \phi}{2\xi_D \kappa \mathbf{q}^2} \left[(1 - e^{-\kappa f_{B'} \mathbf{q}})(1 - e^{-\kappa f_D \mathbf{q}}) \right] \\ S_{DD}(\mathbf{q}) &= \frac{2(1 - \phi)}{\xi_D \kappa \mathbf{q}^2} \left[e^{-\kappa f_D \mathbf{q}} + \kappa f_D \mathbf{q} - 1 \right] \end{aligned} \quad (3.11)$$

where ξ_D is the relative size of the complexed segments, and κ is defined as N_3/N_1 . Derivation of the above Debye functions is omitted, and the reader is encouraged to refer to references²³⁻²⁵ for more details.

Using the \mathbf{S}^0 and \mathbf{X} matrices, which contains the interaction contributions $\chi_{\alpha\beta}$, one could calculate the eigenvalues of the \mathbf{S}^* matrix. The nature of the phase transition is captured by the sign of the smallest eigenvalue of \mathbf{S}^* , here denoted as $\lambda_o(\mathbf{q})$.²¹ If $\lambda_o(\mathbf{q})$ is greater than 0 for all \mathbf{q} , then any small fluctuation increases the free energy. This indicates that the disordered phase is stable. On the other hand if $\lambda_o(\mathbf{q})$ is negative for a certain \mathbf{q}_o , then the disordered phase is unstable. The size of \mathbf{q}_o determines whether the stable phase is due to microscopic or macroscopic fluctuations. Since \mathbf{q} is inversely proportional to length scales in real space, $\mathbf{q}_o = 0$ corresponds to macrophase separation, and finite non-zero $\mathbf{q}_o \neq 0$ corresponds to microphase separation. By analyzing the eigenvalues of \mathbf{S}^* matrix for a set of parameters, the RPA phase diagram can be constructed.

Chapter 4

Numerical Methods

In chapter two a field theoretic model describing complexation in the AB/C system was developed. The solution of that model relied on a self consistent calculation of the propagators, which were used to determine the self-consistent field equations. Setting aside the specifics of the self-consistency algorithm, a numerical technique is required for solving the modified diffusion equations (2.26). There are several numerical techniques for solving differential equations²⁰ (such as the modified diffusion equation considered here), but only two methods are used in this study. Specifically, a method of mean weighted residuals (MWR), known as the Spectral method²⁶ and a finite difference method known as the Alternating Direction Implicit^{27,28} (ADI) are used.

4.1 Reciprocal-Space Method

The reciprocal method is one of several techniques used for minimizing the mean weighted residuals.²⁶ The idea behind this method is to describe the unknown function, the end-integrated propagators in this case, using a set of basis functions which satisfy specific criteria. In general, any unknown function $u(x)$ can be written as

$$u(x) \approx u_N(x) = \sum_{n=0}^N a_n \phi_n(x) \quad (4.12)$$

where $\phi_n(x)$ are the basis functions with coefficients a_n . Given an equation $\mathcal{L}u(x) = f(x)$, with \mathcal{L} being an operator, the residual function is defined as the difference between the approximated and the exact solution.

$$R(x; a_1, a_2, \dots, a_N) = \mathcal{L}u_N(x) - f(x) \quad (4.13)$$

The challenge is to minimize the residual function, where the spectral method is one of several methods used for minimizing $R(x; a_1, a_2, \dots, a_N)$.²⁶

Matsen and Schick were the first to use the spectral method to investigate the phase behavior of block copolymers.²⁹ The spectral method developed here takes advantage of the symmetry and the periodicity of the fields $\phi(\mathbf{r})$ and $\omega(\mathbf{r})$. This means that density and the auxiliary fields can be expanded in the form

$$\begin{aligned} \phi_\alpha(\mathbf{r}) &= \sum_{\mathbf{G}} \phi_\alpha(\mathbf{G}) e^{i\mathbf{G}\cdot\mathbf{r}} \\ \omega_\alpha(\mathbf{r}) &= \sum_{\mathbf{G}} \omega_\alpha(\mathbf{G}) e^{i\mathbf{G}\cdot\mathbf{r}} \end{aligned} \quad (4.14)$$

where $\{\mathbf{G}\}$ are the reciprocal vectors determined by the symmetry of the phase and $\phi_\alpha(\mathbf{G})$ and $\omega_\alpha(\mathbf{G})$ are the Fourier components. The self-consistent field equations can be written in terms of the Fourier basis functions as,¹

$$\begin{aligned}
\frac{\phi_\alpha(\mathbf{G})}{\xi_\alpha} &= \lambda_1 \lambda_{01} \sum_{\mathbf{G}'} \int_0^{f_\alpha} ds q_\alpha(\mathbf{G}', s) q_\alpha^\dagger(\mathbf{G} - \mathbf{G}', f_\alpha - s) \\
\frac{\phi_C(\mathbf{G})}{\xi_C} &= \frac{\lambda_2 \lambda_{02}}{\kappa} \sum_{\mathbf{G}'} \int_0^\kappa ds q_C(\mathbf{G}, s) q_C(\mathbf{G} - \mathbf{G}', \kappa - s) \\
\frac{\phi_\beta(\mathbf{G})}{\xi_\beta} &= \frac{\lambda_1 \lambda_2 \lambda_3 \lambda_{03}}{\kappa'} \sum_{\mathbf{G}'} \int_0^{\kappa' f_\beta} ds q_\beta(\mathbf{G}, s) q_\beta^\dagger(\mathbf{G} - \mathbf{G}', \kappa' f_\beta - s) \\
\frac{\omega_\gamma(\mathbf{G})}{\xi_\gamma} &= \frac{1}{2} \sum_{\gamma \neq \gamma'} \frac{\phi_{\gamma'}(\mathbf{G}) \chi_{\gamma\gamma'}}{\xi_\gamma \xi_{\gamma'}} + \eta(\mathbf{G}) \\
\sum_\gamma \phi_\gamma(\mathbf{G}) &= \delta_{\mathbf{G},0}
\end{aligned} \tag{4.15}$$

The basis functions chosen here are plane waves, which are the appropriate choice given the periodicity of the system. One of the advantages of using the Fourier representation is that the modified diffusion equations which were previously second order differential equation are now first order.

$$\begin{aligned}
\frac{\partial q_\alpha(\mathbf{G}, s)}{\partial s} &= - \sum_{\mathbf{G}'} \mathcal{H}_\alpha(\mathbf{G}, \mathbf{G}') q_\alpha(\mathbf{G}', s) \\
\frac{\partial q_\alpha^\dagger(\mathbf{G}, s)}{\partial s} &= - \sum_{\mathbf{G}'} \mathcal{H}_\alpha(\mathbf{G}, \mathbf{G}') q_\alpha^\dagger(\mathbf{G}', s)
\end{aligned} \tag{4.16}$$

The Hamiltonian $\mathcal{H}_\alpha(\mathbf{G}, \mathbf{G}')$ in the above equation is defined as,¹

$$\mathcal{H}_\alpha(\mathbf{G}, \mathbf{G}') \equiv G^2 \delta_{\mathbf{G}, \mathbf{G}'} + \omega_\alpha(\mathbf{G} - \mathbf{G}') \tag{4.17}$$

To solve the modified diffusion equations (4.16), one could expand the propagators

using a set of basis functions. As it turns out, the eigenfunctions of the Hamiltonian (4.17) are the proper choice for the basis functions. These eigenfunctions can be determined by solving the eigenvalue problem

$$\sum_{\mathbf{G}'} \mathcal{H}_\alpha(\mathbf{G}, \mathbf{G}') \psi_n^\alpha(\mathbf{G}') = \epsilon_n^\alpha \psi_n^\alpha(\mathbf{G}') \quad (4.18)$$

with ϵ_n^α being the eigenvalues of $\mathcal{H}_\alpha(\mathbf{G}, \mathbf{G}')$ Hamiltonian. The eigenfunctions $\psi_n^\alpha(\mathbf{G}')$ form a complete set, with the property

$$\begin{aligned} \sum_{\mathbf{G}'} \psi_n^\alpha(\mathbf{G}') \psi_m^\alpha(\mathbf{G}') &= \delta_{n,m} \\ \sum_n \psi_n^\alpha(\mathbf{G}) \psi_m^\alpha(\mathbf{G}') &= \delta_{\mathbf{G}, \mathbf{G}'} \end{aligned} \quad (4.19)$$

This is due to the Hermitian nature of the Hamiltonian matrix. Solving the eigenvalue equations results in a set of basis functions, which can be used to determine the propagators. This in turn allows one to calculate the SCFE.

The above method can be used for any system with internal symmetry. One could further simplify the calculation by exploring the relationship between vectors in the reciprocal space using the properties of the point group operations. An example would be the set of vectors \mathbf{v}' , determined by applying the point group operations on a general vector \mathbf{v} in the reciprocal space. The vectors \mathbf{v}' form a set known as the *star* of \mathbf{v} . This means that the vectors within one star are related to one another. Using this idea, the plane wave expansion introduced earlier can be modified to utilize the relationship between the vectors in a star.¹ A new set of basis functions, each being

a linear combination of vectors within one star, can be constructed.

$$f_n(\mathbf{r}) = \frac{1}{\sqrt{N_n}} \sum_{i \in n} S_i^n e^{i\mathbf{G}_i^n \cdot \mathbf{r}} \quad (4.20)$$

In the above equation, the summation is over all the vectors within a star, denoted by n , with N_n being the number of the vectors. The factors S_i^n take on values of $+1$ or -1 according to the space group.¹ These basis functions are the linear combination of the plane waves. They form an orthogonal set, satisfying the eigenvalue equation,

$$\nabla^2 f_n(\mathbf{r}) = -\lambda_n f_n(\mathbf{r}) \quad (4.21)$$

with ∇^2 being the Laplacian operator. In terms of the new basis functions the Hamiltonian (4.17) can be written as,¹

$$\mathcal{H}_{n,m}^\alpha \equiv \lambda_n \delta_{n,m} + \sum_l \Gamma_{n,m,l} \omega_l^\alpha \quad (4.22)$$

where,

$$\begin{aligned} \Gamma_{n,m,l} &= \frac{1}{V} \int d\mathbf{r} f_n(\mathbf{r}) f_m(\mathbf{r}) f_l(\mathbf{r}) \\ &= \frac{1}{\sqrt{N_n N_m N_l}} \sum_{i \in n} \sum_{j \in m} \sum_{k \in l} S_i^n S_j^m S_k^l \delta_{\mathbf{G}_i^n + \mathbf{G}_j^m + \mathbf{G}_k^l, \mathbf{0}} \end{aligned} \quad (4.23)$$

The eigenvalue equation (4.18) still holds, but now with the Hamiltonian defined by equation (4.22). The self consistent-field equations can also be written in terms of the new basis functions. Solving the eigenvalue problem (4.21) allows one to calculate the self-consistent field equations and the free energy. In terms of the eigenfunctions,

the end-integrated propagators can be written as

$$\begin{aligned}
q_n^\alpha(s) &= \sum_i e^{-\epsilon_i^\alpha s} \psi_{1,i}^\alpha \psi_{n,i}^\alpha \\
q_n^{\alpha\dagger}(s) &= \sum_{i,j} e^{-\epsilon_i^\alpha s} \psi_{n,i}^\alpha \left[\sum_m \psi_{m,i}^\alpha \psi_{m,j}^\beta \right] e^{-\epsilon_j^\beta s} \psi_{1,j}^\beta
\end{aligned} \tag{4.24}$$

where the self-consistent field equations are then expressed in the following form

$$\begin{aligned}
\frac{\phi_\alpha^n}{\xi_\alpha} &= \lambda_1 \lambda_{01} \sum_{m,l} \int_0^{f_\alpha} ds \Gamma_{n,m,l} q_m^\alpha(s) q_l^{\alpha\dagger}(f_\alpha - s) \\
\frac{\phi_C^n}{\xi_C} &= \frac{\lambda_2 \lambda_{02}}{\kappa} \sum_{m,l} \int_0^\kappa ds \Gamma_{n,m,l} q_m^C(s) q_l^C(\kappa - s) \\
\frac{\phi_\beta^n}{\xi_\beta} &= \frac{\lambda_1 \lambda_2 \lambda_3 \lambda_{03}}{\kappa'} \sum_{m,l} \int_0^{\kappa' f_\beta} ds \Gamma_{n,m,l} q_m^\beta(s) q_l^{\beta\dagger}(\kappa' f_\beta - s) \\
\frac{\omega_\gamma^n}{\xi_\gamma} &= \frac{1}{2} \sum_{\gamma \neq \gamma'} \frac{\phi_{\gamma'}^n \chi_{\gamma\gamma'}}{\xi_\gamma \xi_{\gamma'}} + \eta^n \\
\sum_\gamma \phi_\gamma^n &= \delta_{n,0}
\end{aligned} \tag{4.25}$$

The above equations are solved self-consistently until a given numerical convergence criteria is reached.

4.2 Alternating Direction Implicit Method

In this section, the Alternating Direction Implicit (ADI) technique is described. This method is specially powerful when considering parabolic equations on rectangular domains.³⁰ ADI is a finite difference technique, which relies on the splitting of the spatial marching into two steps. The first step is implicit along one axis and explicit along the other, and vice versa for the second step. The alternate marching

is carried out for each temporal¹ step.²⁸ Although the ADI method is mostly used for two dimensional systems, it has been extended to three dimensions. The 3-D ADI is much more tedious, and thus its application to two dimensional systems has been considered here.

The ADI technique is used to solve the modified diffusion equation,

$$\frac{\partial}{\partial s} q(\mathbf{r}, s) = R_g^2 \nabla^2 q(\mathbf{r}, s) - \omega(\mathbf{r})q(\mathbf{r}, s) \quad (4.26)$$

where the Laplacian operator ∇^2 assumes different forms, depending on the type of the coordinate system chosen. The parameters α and \dagger used in equation (2.26) are dropped for simplicity. Since the ADI method considered here captures the physics of a two dimensional system, with self-consistent equations being homogenous in the third dimension, it is important to consider the symmetry of the structures formed. For example, the equations describing the lamellar structure are homogenous in two dimension and vary along the dimension perpendicular to the lamellar interface. For the sake of generality, the ADI technique is described in the cylindrical coordinate system. This formalism can then be easily modified to capture the physics in planar geometry. The end-integrated propagators are assumed to be invariant along the θ axis and vary in the r and z directions.

¹It is important to recognize that for the modified diffusion equation, time is replaced by the segment number along the chain.

Within this framework, the modified diffusion equation becomes,

$$\frac{\partial}{\partial s}q(r, z, s) = R_g^2 \left[\frac{\partial^2}{\partial r^2} + \frac{\partial}{r \partial r} + \frac{\partial^2}{\partial z^2} \right] q(r, z, s) - \omega(r, z)q(r, z, s) \quad (4.27)$$

where the length scales are normalized with respect to R_g^2 , by setting $R_g^2 = 1$. A simulation box of size $N \times N$, with unit grid of size $\Delta r \times \Delta z$ is considered. Indices i and j are introduced to represent the r and z axis. Using the modified ADI method, the modified diffusion equation in two half time steps becomes,³¹

$$\begin{aligned} & \left[-\frac{\Delta s}{2 \Delta r^2} + \frac{\Delta s}{(i \Delta r + r_o)4 \Delta r} \right] q_{i-1,j}^{s+1} + \left[1 + \frac{\Delta s}{\Delta r^2} + \frac{\Delta s \omega_{i,j}}{2} \right] q_{i,j}^{s+1} + \left[-\frac{\Delta s}{2 \Delta r^2} - \frac{\Delta s}{(i \Delta r + r_o)4 \Delta r} \right] q_{i+1,j}^{s+1} \\ = & \left[\frac{\Delta s}{2 \Delta z^2} \right] q_{i,j-1}^s + \left[1 - \frac{\Delta s}{\Delta z^2} \right] q_{i,j}^s + \left[\frac{\Delta s}{2 \Delta z^2} \right] q_{i,j+1}^s \end{aligned} \quad (4.28)$$

solved implicitly in the r direction and explicitly in the z and,

$$\begin{aligned} & \left[-\frac{\Delta s}{2 \Delta z^2} \right] q_{i,j-1}^{s+1} + \left[1 + \frac{\Delta s}{\Delta z^2} \right] q_{i,j}^{s+1} + \left[-\frac{\Delta s}{2 \Delta z^2} \right] q_{i,j+1}^{s+1} \\ = & \left[\frac{\Delta s}{2 \Delta r^2} - \frac{\Delta s}{(i \Delta r + r_o)4 \Delta r} \right] q_{i-1,j}^s + \left[1 - \frac{\Delta s}{\Delta r^2} - \frac{\Delta s \omega_{i,j}}{2} \right] q_{i,j}^s + \left[\frac{\Delta s}{2 \Delta r^2} + \frac{\Delta s}{(i \Delta r + r_o)4 \Delta r} \right] q_{i+1,j}^s \end{aligned} \quad (4.29)$$

solved implicitly in the z direction and explicitly in the r . The above set of equations will be solved using an iterative algorithm for all i and j , with the convergence condition $\Delta s \leq (\Delta r \Delta z)/4$.

A more friendly way of writing the above set of equations is by using matrices. For the forward step in the i direction, Eq.(4.28) becomes;

$$\begin{bmatrix} \beta_{1,j} & (\alpha^* + \alpha) & 0 & \dots & 0 \\ \alpha & \beta_{2,j} & \alpha^* & \dots & 0 \\ 0 & \cdot & \dots & \cdot & \cdot \\ \cdot & \cdot & \dots & \cdot & \cdot \\ \cdot & \cdot & \alpha & \beta_{N-1,j} & \alpha^* \\ 0 & \cdot & \cdot & (\alpha^* + \alpha) & \beta_{N,j} \end{bmatrix} \begin{bmatrix} q_{1,j}^{s+1} \\ q_{2,j}^{s+1} \\ \cdot \\ \cdot \\ \cdot \\ q_{N,j}^{s+1} \end{bmatrix} = \begin{bmatrix} \gamma q_{1,j-1}^s + \sigma q_{1,j}^s + \gamma q_{1,j+1}^s \\ \gamma q_{2,j-1}^s + \sigma q_{2,j}^s + \gamma q_{2,j+1}^s \\ \cdot \\ \cdot \\ \cdot \\ \gamma q_{N,j-1}^s + \sigma q_{N,j}^s + \gamma q_{N,j+1}^s \end{bmatrix}$$

and similarly Eq.(4.29) can be written as,

$$\begin{bmatrix} \sigma & 2\gamma & 0 & \dots & 0 \\ \gamma & \sigma & \gamma & \dots & 0 \\ 0 & \cdot & \dots & \cdot & \cdot \\ \cdot & \cdot & \dots & \cdot & \cdot \\ \cdot & \cdot & \gamma & \sigma & \gamma \\ 0 & \cdot & \cdot & 2\gamma & \sigma \end{bmatrix} \begin{bmatrix} q_{i,1}^{s+1} \\ q_{i,2}^{s+1} \\ \cdot \\ \cdot \\ \cdot \\ q_{i,N}^{s+1} \end{bmatrix} = \begin{bmatrix} \alpha q_{i-1,1}^s + \beta_{i,1} q_{i,j}^s + \alpha^* q_{i+1,1}^s \\ \alpha q_{i-1,2}^s + \beta_{i,2} q_{i,2}^s + \alpha^* q_{i+1,2}^s \\ \cdot \\ \cdot \\ \cdot \\ \alpha q_{i-1,N}^s + \beta_{i,N} q_{i,N}^s + \alpha^* q_{i+1,N}^s \end{bmatrix}$$

It is important to adjust the array on the right hand side for the edges of the box, where zero flux boundary condition must be satisfied. The above matrix equations must be solved for $s = 0$ to $s = N_\alpha$, once for each propagator. The solutions to the forward propagator q is used as the initial condition for the complementary propagator q^\dagger . After calculating the propagators, the self-consistent field equations and the free energy, can be determined. This process is repeated until some convergence condition is met.

Although the ADI technique is computationally slower and less accurate than the spectral method, it assumes no underlying initial symmetry. The advantage of the ADI technique is that it provides a real space solution for a given set of parameters and can be used for studying non-periodic structures. There are other computationally more efficient and accurate numerical techniques with real space flexibility. One of such techniques, is the pseudospectral method.²⁶ This method provides an accurate and efficient way for calculating the properties of complex and simple structures. The spectral method used in this work is computationally more efficient than the pseudospectral technique. On similar note, if 2-D solutions to the modified diffusion equation are required, the ADI technique provides a faster but less accurate way, in comparison to the pseudospectral method, for calculating the phase behavior of the system.

Chapter 5

Results and Discussion

Using the numerical techniques presented in chapter 4, the SCFT model developed in chapter 2 will be investigated. A system containing n_1 diblock copolymers, n_2 homopolymers and n_3 complexed polymer chains in volume V is considered. The relative length of the homopolymer and complexed chains are measured with respect to the length of the diblock chain, with $N_2/N_1=0.5$ and $N_3/N_1=1$. The length of the diblock chain is defined by $N_A = f_A N_1$ and $N_B = f_B N_1$ where f_A and f_B are the fraction of the A and B segments, respectively. Although the calculations are carried out with the grand canonical ensemble, the phase diagrams are represented in terms of the homopolymer volume fraction ϕ_H .

The purpose of this thesis is to examine the validity of the interpolymer complexation and the attractive interaction models for studying hydrogen-bonding in (AB) diblock copolymer/ (C) homopolymer blends. Hydrogen-bonding is assumed to be between the A and C monomers. In the attractive interaction model, details of which

can be found in ref [2], hydrogen-bonding is modeled by a negative interaction parameter ($-\chi$). In this model, one could adjust the strength of hydrogen-bonds by the relative magnitude of the χ parameter. In contrast, the interpolymer complexation model treats hydrogen-bonding as a complexation process, in which monomers with hydrogen-bonding capability are considered as donor/ acceptor sites. Figure [5.1] shows a schematic representation of this model.

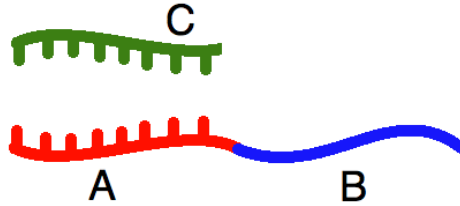


Figure 5.1: Schematic diagram for AB/C complexation, where the C homopolymer is capable of hydrogen-bonding with A block of the diblock copolymer.

In the first section of this chapter, the phase behavior of the attractive interaction model is investigated using the RPA and SCFT, followed by analysis of interpolymer complexation model in section two.

5.1 The Attractive Interaction Model

In this section, the phase behavior of the system in the $f_A-\phi_H$ and $\chi_{AC}-\phi_H$ plane is obtained. A mixture of AB diblock copolymers and C homopolymers results in a

large parameter space. These parameters are the interactions χ_{AB} , χ_{AC} and χ_{BC} , the fraction length of A in diblock (f_A), the relative polymerization of the C chain (κ) and the volume fraction of the homopolymers (ϕ_H). Using SCFT to explore these parameters would be computationally expensive, and thus the first step is to investigate the phase space using the computationally less expensive RPA technique. Using the method developed in section three, the order-disorder transition (ODT) lines are calculated.

Figure [5.2] shows the RPA phase diagram for a blend with $\chi_{AB} = 12$, $\chi_{AC} = -10$, $\chi_{BC} = 15$ and $\kappa = 0.5$ in the f_A - ϕ_H plane. The phase diagram shows both order-to-disorder ($f_A \gtrsim 0.25$) and 2-phase-to-disorder ($f_A \lesssim 0.25$) phase transitions. The 2-phase region is a macrophase separated state with diblock rich/ homopolymer rich macroscopic domains. Using the RPA technique, only the stability of the homogeneous phase is captured, and no information about the phase transitions within the microphase separated and 2-phase regions can be determined. Macrophase separation of the homopolymer and diblock chains is expected since there is a large positive (repulsive) interaction between the B and C monomers. This means that for small f_A values, the system is driven into a 2-phase region with increase in ϕ_H . The negative interaction parameter between the A and C monomers (χ_{AC}) indicates the miscibility of C homopolymers in the AB blend. The pure AB diblock copolymer with $\chi_{AB} = 12$, $\phi_H = 0$ and $f_A = 0.5$ assumes the lamellar morphology²⁹. It is interesting to investigate the effect of the addition of the C homopolymers on this structure. The phase diagram [5.2] suggests an order-to-disorder phase transition at relatively high values of ϕ_C , in an AB/C blend with $f_A = 0.5$. Although details of the phase transitions

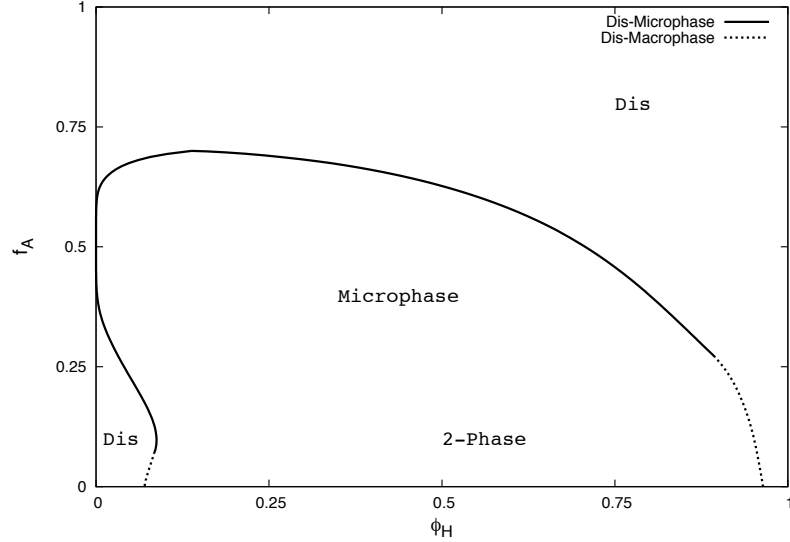


Figure 5.2: RPA phase diagram for blends with parameters $\chi_{AB} = 12, \chi_{AC} = -10, \chi_{BC} = 15$ and $\kappa = 0.5$. The 2-phase region is a macrophase separated state with diblock rich/ homopolymer rich macroscopic domains.

within the microphase domain can not be resolved using the RPA, order-order phase transitions are expected.

To investigate the effect of hydrogen-bonding strength on the phase behavior of the AB/C blends, order-disorder transition lines in the $\chi_{AC}-\phi_H$ plane are calculated. Figure [5.3] shows the RPA phase diagram for the system with $\chi_{AB} = 12, \chi_{BC} = 15, f_A = 0.5$ and $\kappa = 0.5$ in the $\chi_{AC}-\phi_H$ plane. Order-to-disorder ($\chi_{AC} \gtrsim -2$) and 2-phase-to-disorder ($\chi_{AC} \lesssim -2$) phase transitions are also observed in this case. For blends with $\chi_{AC} \gtrsim -2$, increasing the diblock copolymer concentration in an otherwise homogenous homopolymer rich system results in disorder-to-order phase transition.

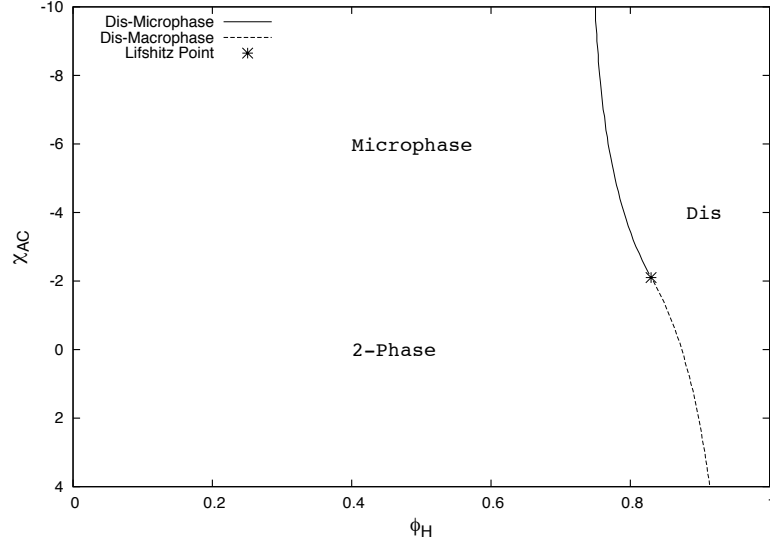


Figure 5.3: RPA phase diagram for blends with parameters $\chi_{AB} = 12, \chi_{BC} = 15, f_A = 0.5$ and $\kappa = 0.5$.

On the other hand, for blends with $\chi_{AC} \lesssim -2$, transition from disordered into 2-phase region is observed. Since χ_{AB} is greater than 10.5 and $f_A = 0.5$, blends with ϕ_H of approximately zero form lamellar structure. The RPA calculation indicates that for blends with $\chi_{AC} \gtrsim -2$, there is a possibility of order-order phase transitions. Determining the details within the microphase separated region is beyond the RPA calculations, and SCF solutions are required for further investigation.

We now turn to the results from the SCFT calculations. The solutions to the modified diffusion equations (2.26) were obtained using the spectral method⁴ for the classical lamellar (Lam), cylindrical (Hex) and spherical (BCC) structures. The

phase behavior within the microphase separated regions predicted by the RPA technique is studied. Figure [5.4] is the SCF phase diagram calculated for the AB/C system with parameters similar to that in Figure [5.2]. As indicated previously in the RPA phase diagram, the AB/C blend is driven from the disorder phase into a 2-phase region when ϕ_H is increased. For blends with $0.25 \lesssim f_A \lesssim 0.3$, increase in the homopolymer concentration results in disorder \rightarrow order \rightarrow disorder phase transitions. The microphase separated region shows order-order phase transitions from

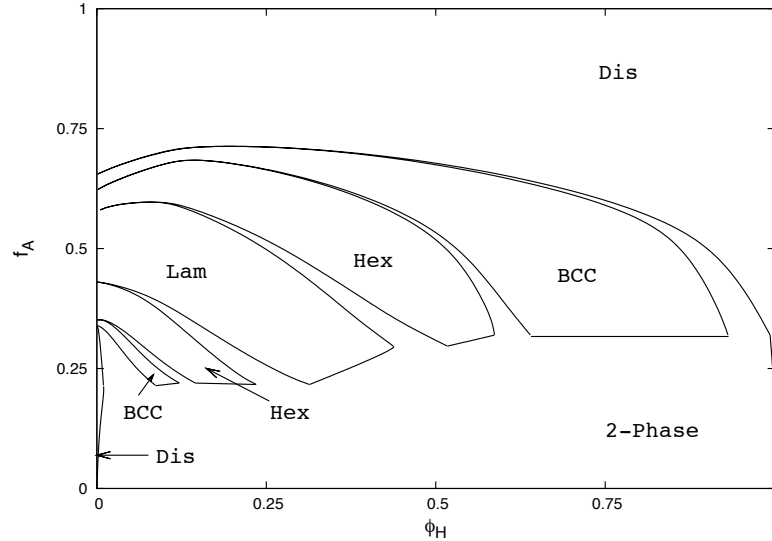


Figure 5.4: The phase diagram for the AB/C blend with $\chi_{AC} = -10$, $\chi_{BC} = 15$, $\chi_{AB} = 12$ and $\kappa = 0.5$. Disordered, Microphase separated and two phase regions are observed. In the microphase region, Lamellar (lam), Cylindrical (Hex) and Spherical (BCC) phases are shown.

$BCC_A \rightarrow Hex_A \rightarrow Lam \rightarrow Hex_B \rightarrow BCC_B$. The subscript A means an A rich core in a B

rich matrix and vice versa for subscript B . The phase behavior observed here resembles that of a pure AB diblock blend.²⁹ This indicates that the attractive interaction between the A and C monomers has the same effect as increasing f_A in a pure AB system. The phase transition sequences observed for the AB/C blends with f_A of 0.5 is consistent with experiments.¹⁰ Starting with a pure lamellar phase separated AB blend, Chen et al.¹⁰ showed that increasing the homopolymer concentration results in Lam \rightarrow Hex \rightarrow BCC \rightarrow Dis phase transitions for strong hydrogen-bonding. They also showed a Lam \rightarrow 2-phase phase transition with increase in ϕ_H for weak hydrogen-bonding. The phase transition sequences observed by Chen et al.¹⁰ is consistent with those shown in Fig[5.5]. The order-order phase transitions shown for $\chi_{AC} < -2$ is consistent with those observed for strong hydrogen-bonding. Similarly, the order-to-2-phase phase transition for $\chi_{AC} > -2$ is consistent with the phase transition observed experimentally.¹⁰

As mentioned, the strength of hydrogen-bonds is assumed to be modeled by the relative magnitude of the χ_{AC} parameter. It is interesting to investigate the results described by Chen and coworkers¹⁰ by exploring the phase behavior in the χ_{AC} - ϕ_H plane. Figure [5.5] shows the SCF phase diagram for the AB/C blend with parameters similar to that in Fig [5.3]. The phase behavior of the blends with $\chi_{AC} \gtrsim -4$ resembles those seen experimentally for blends with strong hydrogen-bonding. Similarly, increasing the homopolymer concentration in blends with $\chi_{AC} \lesssim -2$ results in an order-to-2-phase phase transition. This indicates that weak hydrogen-bonding enhances the miscibility only for small concentrations of the C homopolymer.

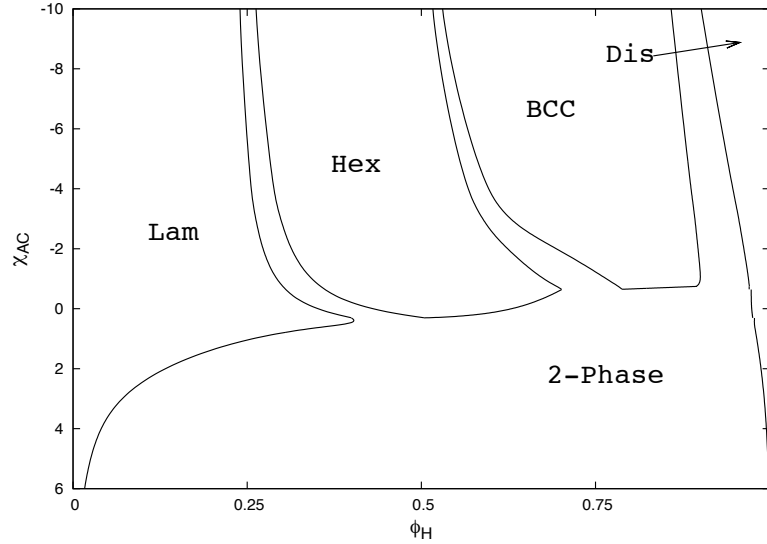


Figure 5.5: Phase diagram for the AB/C blend with $\chi_{AB} = 12$, $\chi_{BC} = 15$, $f_A = 0.5$ and $\kappa = 0.5$.

The observations indicate that the phase behavior predicted by the attractive interaction model is in qualitative agreement with experiments.¹⁰ To further validate the model, the effect of homopolymer concentration on the lamellar domain spacing is investigated. The lamellar spacing is the period of the lamellar structure. Figure [5.6] shows the normalized lamellar spacing for two blends, one modeling strong-hydrogen bonding (the dotted-line) and the other modeling weak hydrogen-bonding (solid line). It is evident that increase in the homopolymer concentration results in an increase in the lamellar spacing for both strong and weak hydrogen-bonding. To further understand the cause of this increase, density profiles for both blends are plotted. Figure [5.7] shows the density profiles for blends with $\chi_{AB} = 12$, $\chi_{BC} = 15$, $f_A = 0.5$, $\kappa = 0.5$

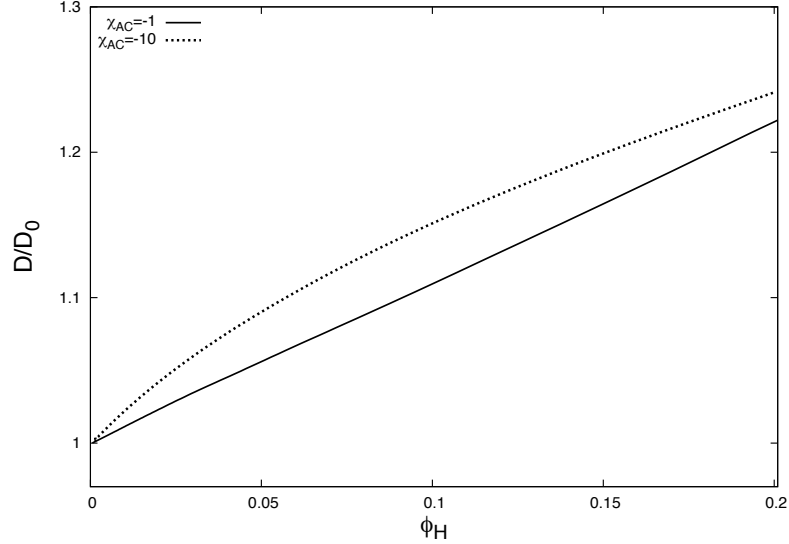


Figure 5.6: Normalized lamellar spacing for the AB/C system with $\chi_{AB} = 12$, $\chi_{BC} = 15$, $f_A = 0.5$, $\kappa = 0.5$ and $\chi_{AC} = -10$ (dotted line) and $\chi_{AC} = -1$ (solid line).

and $\chi_{AC} = -10$ (dotted line) and $\chi_{AC} = -1$ (solid line) for ϕ_H of 20%. The attractive interaction between the A and C monomers results in the aggregation of the C segments in the A rich domains. Since the A and C segments are not chemically bonded, it is energetically and entropically more favorable for the C monomers to aggregate away from the B rich domains, resulting in the increase in the lamellar spacing shown in Fig[5.6]. To better understand the results captured in Fig[5.6] and [5.7], a schematic diagram showing the increase in the lamellar spacing due the homopolymer concentration is constructed. Figure [5.8 a] shows the lamellar structure with 0% ϕ_H . The initial lamellar domain spacing of this structure is taken as reference. Figure [5.8 b] shows the lamellar structure with a finite amount of homopolymer additive. The

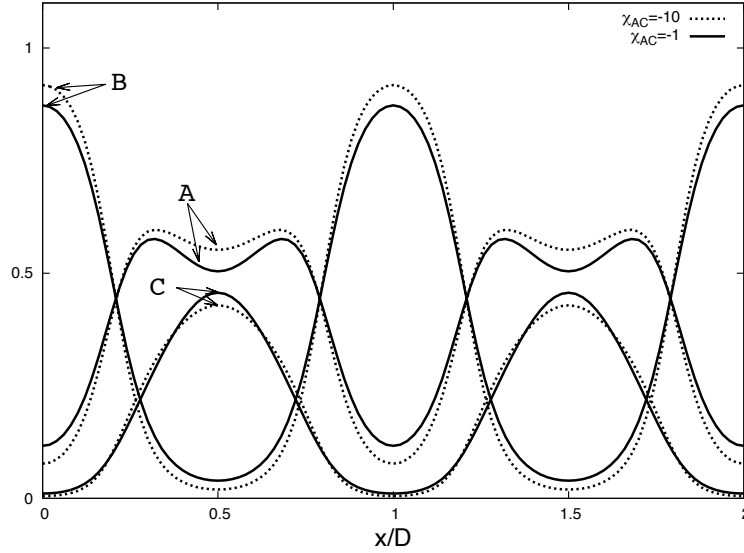


Figure 5.7: Density profile for the AB/C system, with $\chi_{AB} = 12$, $\chi_{BC} = 15$, $f_A = 0.5$, $\kappa = 0.5$ and $\chi_{AC} = -10$ (dotted line) and $\chi_{AC} = -1$ (solid line). ϕ_H is 20% for both blends. The x axis is the axis perpendicular to the lamellar interface, normalized with respect to the lamellar domain spacing.

homopolymer chains have aggregated at the A rich domain for the reasons mentioned in the above paragraph. At the first glance, it seems energetically favorable for the C chains to completely wet the lamellar structure, since there is an attractive interaction between the A and C segments. Wetting the lamellar structure reduces the entropic energy for both diblock and homopolymer chains. This can be understood, since the wetting process reduces the configurational states available to chains. The homopolymers are forced to concentrate in the region between the lamellar sheets, thus increasing the lamellar domain spacing.

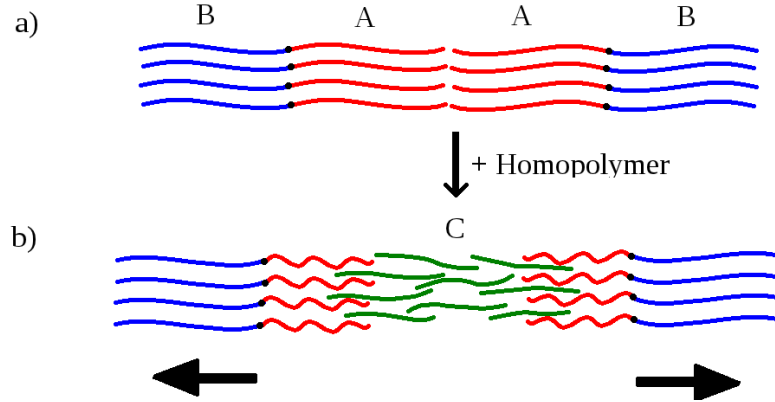


Figure 5.8: Density profile for the AB/C system, with $\chi_{AB} = 12$, $\chi_{BC} = 15$, $f_A = 0.5$, $\kappa = 0.5$ and $\chi_{AC} = -10$ (dotted line) and $\chi_{AC} = -1$ (solid line). ϕ_H is 20% for both blends.

The lamellar spacing behavior predicted by the attractive interaction model for strong hydrogen-bonding is not consistent with experiments. In particular, Chen and coworkers have observed a decrease in the lamellar spacing with an increase of the homopolymer concentration.¹⁰ As illustrated in the density profiles, the nature of the interactions between the monomers demands an increase in the lamellar spacing. In other words, the fact that A and C monomers are not chemically bonded leads to a segregation of the C -homopolymers in the middle of the A -domains, thus always resulting in an increase in the lamellar spacing. This observation demonstrates that, although the attractive interaction model provides qualitatively correct phase transition sequences, this model is not adequate model for hydrogen-bonding systems.

5.2 The Interpolymer Complexation Model

Although the attractive interaction model captures the qualitative phase behavior of hydrogen-bonded AB/C blends, it fails to predict the correct changes in the lamellar domain spacing. The results presented in the previous section indicate that an attractive interaction model does not capture the physics of hydrogen-bonding. As shown previously in this and earlier chapters, the interpolymer complexation model assumes physical bonding between monomers with hydrogen-bonding capabilities. The SCFT model developed in chapter two allows for a complexation of type $AB+C \rightleftharpoons A'B'C'D$, where only linear complexation is allowed for simplicity. A problem which arises when considering such model is the complexity of structures formed as the result of the complexation process. Figure [5.9] shows some of these complex structures. The architecture and fraction of these supramolecular chains are determined by considering the chemical equilibrium of the system. The equilibrium occurs when, $\mu_1 + \mu_2 = \mu_3$, where μ_1 , μ_2 and μ_3 are the chemical potential of diblock copolymer, homopolymer and complexed polymer chains, respectively. Using the mass actions formalism¹⁹, one could determine the equilibrium fraction of the complexed chains. The mass action formalism for the homogenous phase results in

$$\frac{1 - \bar{\phi}_s}{\sigma\theta\bar{\phi}_s^2} = \frac{\kappa'}{\kappa N_1 \rho_o} \frac{Q_3}{Q_1 Q_2} \quad (5.30)$$

Solutions to equation (5.30) can be determined graphically by plotting both sides of the equation with respect to the volume fraction of the single-stranded chains $\bar{\phi}_s$. The solutions to the equation (5.30) are analyzed with respect to the strength and number of hydrogen-bonds. This is done by changing ϵ (the strength of individual

hydrogen-bonds) and κ' (number of hydrogen-bonds).

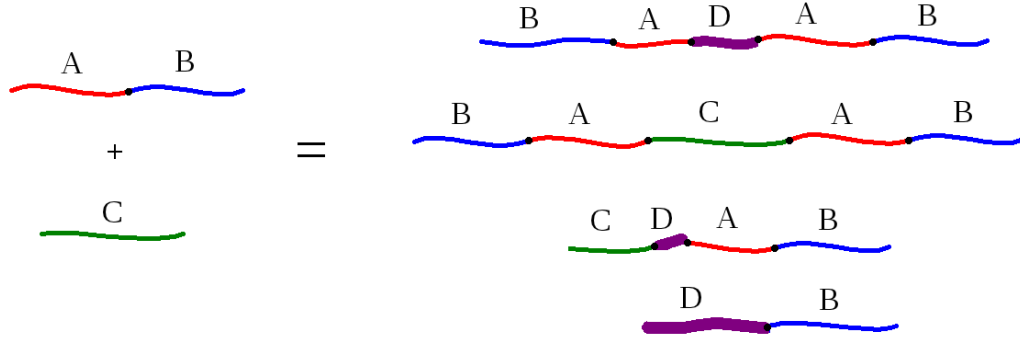


Figure 5.9: Schematic diagram showing a few examples of what could result from a linear complexation. In this model, D segments are the result of the complexation of the A and C monomers.

Figure [5.11] shows the solutions to the mass action equation for the system with $\chi_{AB} = 20$, $\chi_{AC} = \chi_{BC} = \chi_{AD} = \chi_{CD} = 5$, $\chi_{BD} = 25$, $f_A = 0.5$, $\kappa = 0.5$, $\kappa' = 1$ and $\xi_D = 2$ for strong (solid line), intermediate (dotted line) and weak (dashed line) hydrogen-bonding. The solutions indicate that for a homogenous mixture, strong hydrogen-bonding results in a complexation of $AB + C \rightleftharpoons B'D$. This result is expected, because it is energetically more favorable for the complexation to result in a $B'D$ structure. To determine the architecture of the complexed $A'B'C'D$ chains, the solutions to the mass action equation are analyzed for different κ' values. Figure [5.10] shows the solutions for the system with $\chi_{AB} = 20$, $\chi_{AC} = \chi_{BC} = \chi_{AD} = \chi_{CD} = 5$, $\chi_{BD} = 25$, $f_A = 0.5$, $\kappa = 0.5$, and $\xi_D = 2$ for a fixed hydrogen-bonding strength (ϵ).

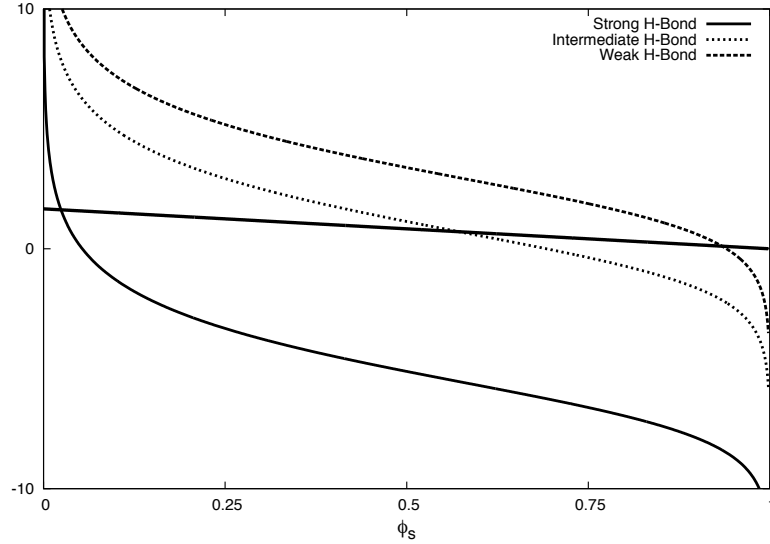


Figure 5.10: Graphical representation of solutions to equation (5.30) for the AB/C blends with $\chi_{AB} = 20$, $\chi_{AC} = \chi_{BC} = \chi_{AD} = \chi_{CD} = 5$, $\chi_{BD} = 25$, $f_A = 0.5$, $\kappa = 0.5$, $\kappa' = 1$ and $\xi_D = 2$. Solid, dashed and dotted lines represent strong, intermediate and weak hydrogen bonding (ϵ).

Larger values of κ' correspond to smaller overlaps between the AB and C chains. In other words, when $\kappa' = 1$, $AB+C$ results in a complete complexation. The solid, dashed and dotted lines in Fig[5.11] show that for a fixed hydrogen-bonding strength, complete complexation is energetically most favorable. The results from Fig [5.10] and [5.11] indicate that when considering complexation in the strong hydrogen-bonding limit, the reaction $AB+C=B'D$ is most dominant. It is important to point out that the complexed monomers were assumed to occupy twice the volume of the single stranded monomers.

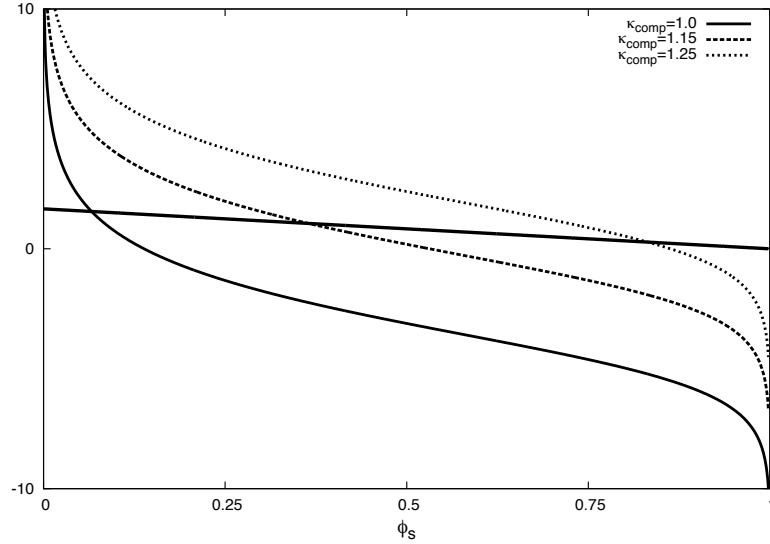


Figure 5.11: Graphical representation of the solutions to equation (5.30) for the AB/C blends with $\chi_{AB} = 20$, $\chi_{AC} = \chi_{BC} = \chi_{AD} = \chi_{CD} = 5$, $\chi_{BD} = 25$, $f_A = 0.5$, $\kappa = 0.5$, and $\xi_D = 2$, where ϵ is fixed and the number of hydrogen-bonding sites controlled by κ' is varied.

To investigate the phase behavior of AB/C blend at the strong hydrogen-bonding limit, the modified diffusion equations (2.26) were solved for the AB/B'D system. For simplicity it is assumed that the complexation process is complete and symmetric, meaning $A+C=D$. It is important to account for physical changes to the structure of the complexed polymers. In other words, changes to the thickness of the complexed chains must be considered. To investigate the effect of chain thickness on the phase behavior of the system, phase diagrams were constructed in the ξ_D - ϕ_H plane using RPA and SCFT. Figure [5.12] shows the RPA phase diagram for the AB/B'D system with $\chi_{AB} = 15$, $\chi_{AD} = 5$, $\chi_{BD} = 17$ and $f_A = f_D = 0.5$. Here ϕ_H corresponds to

the volume fraction of hydrogen-bonded chains. An order-to-disorder phase transi-

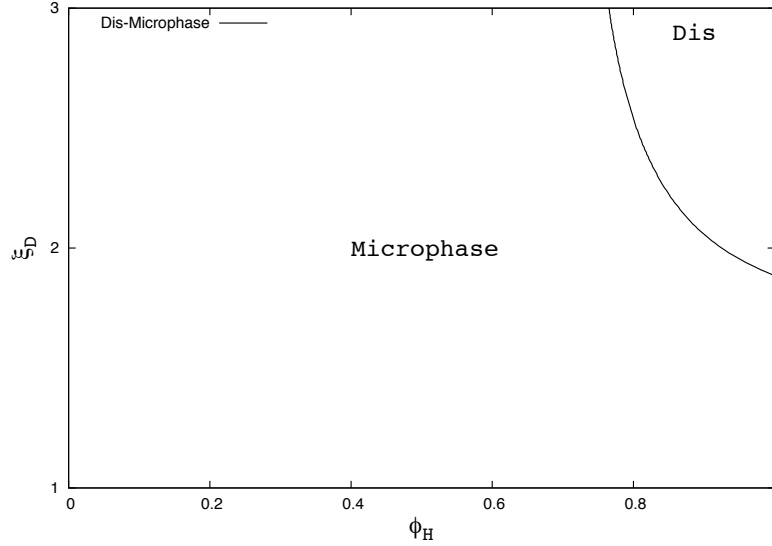


Figure 5.12: RPA phase diagram for the $AB/B'D$ system with $\chi_{AB} = 15$, $\chi_{AD} = 5$ and $\chi_{BD} = 17$ with $f_A = f_D = 0.5$.

tion is observed for blends with $\xi_D \gtrsim 1.8$. This indicates that the phase transition is caused by the asymmetry in the chain thickness. The AB and $B'D$ blends with $\xi_D = 1$, form lamellar structure. This means that increase in ϕ_H (complexed chains) does not result in a phase transition. On the other hand, for $\xi_D = 2$, the pure $B'D$ blend is disordered, whereas the pure AB blend forms a lamellar structure. In this scenario, increase in the concentration of the complexed polymers ($B'D$) results in an order-to-disorder phase transition. Within the microphase region, order-order phase transitions are speculated.

Using SCFT a phase diagram for a system with parameters similar to that in Fig [5.12] is constructed. Figure [5.13] shows that an increase of ϕ_H results in order-order phase transitions for blends with $\xi_D \gtrsim 1.5$. In blends with $\xi_D = 2$, increase in the ϕ_H results in Lam \rightarrow Hex \rightarrow BCC \rightarrow Dis phase transitions. These results indicate the importance of accounting for thickness asymmetry in the complexation model. The phase behavior observed here is consistent with experiments¹⁰ and the attractive interaction model in the strong hydrogen-bonding limit.

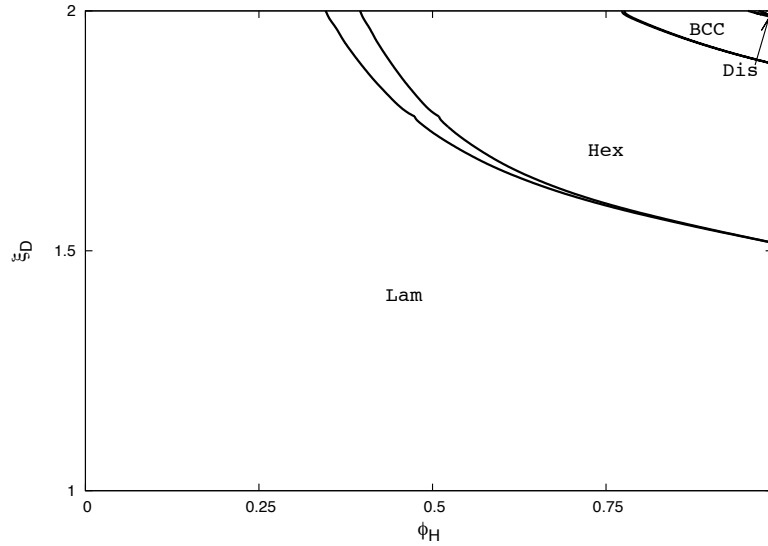


Figure 5.13: Phase diagram for the $AB/B'D$ system with $\chi_{AB} = 15$, $\chi_{DB} = 17$ and $\chi_{AD} = 5$. Both chains are symmetrical and of equal length. Here the subscript H in ϕ_H means the hydrogen-bonded chains.

To further study the effectiveness of the interpolymer complexation for modeling hydrogen-bonding, the effect of ϕ_H on the lamellar domain spacing was investigated.

Figure [5.14] shows the lamellar spacing calculated for the $AB/B'D$ system with $\chi_{AB} = 15$, $\chi_{DB} = 17$, $\chi_{AD} = 5$ and $\xi_D=2$. It shows that increase in the concentration of hydrogen-bonded chains (ϕ_H) results in a decrease in the lamellar spacing. The shrinking in the lamellar spacing can be related to the thickness asymmetry in the chains. To prove this, the lamellar spacing in an $AB/A'B'$ blend is calculated. The AB and $A'B'$ chains are chemically identical, thus $\chi_{AA'}$ and $\chi_{BB'}$ are set to zero. The A' monomers are chosen to be 25% larger than other species, to isolate for the effect of thickness asymmetry on the lamellar spacing. Figure [5.15] shows the

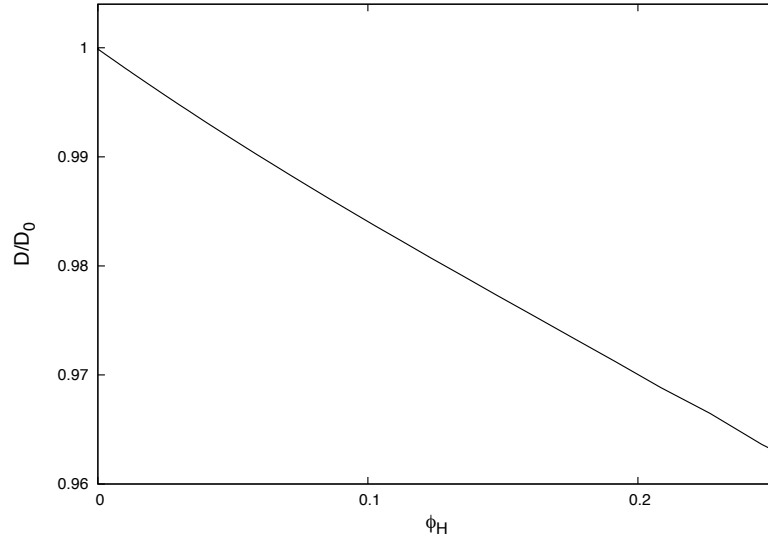


Figure 5.14: Normalized lamellar spacing for the $AB/B'D$ system with $\chi_{AB} = 15$, $\chi_{DB} = 17$, $\chi_{AD} = 5$ and $\xi_D=2$.

change in lamellar spacing with respect to ϕ_H ($\phi_{A'B'}$) for an $AB/A'B'$ system with $\chi_{AB} = \chi_{A'B'} = 13$ and $\xi_{A'}=1.25$. It is clear that an increase in $\phi_{A'B'}$ results in a

decrease in the lamellar spacing. This result can be interpreted in the following way. In a symmetrical AB diblock chain, the volume occupied by the A and B monomers is the same. After complexation, the volume occupied by the complexed monomers (A') is increased. The effect of the asymmetry in the total volume of the chain is countered by the shrinking of the B chains toward the lamellar interface. This can be shown explicitly by calculating the A, A', B and B' segment lengths individually. Figure [5.16] shows the result of this analysis, where the segment lengths are normalized with respect to their initial values. These results indicate that the thick A'

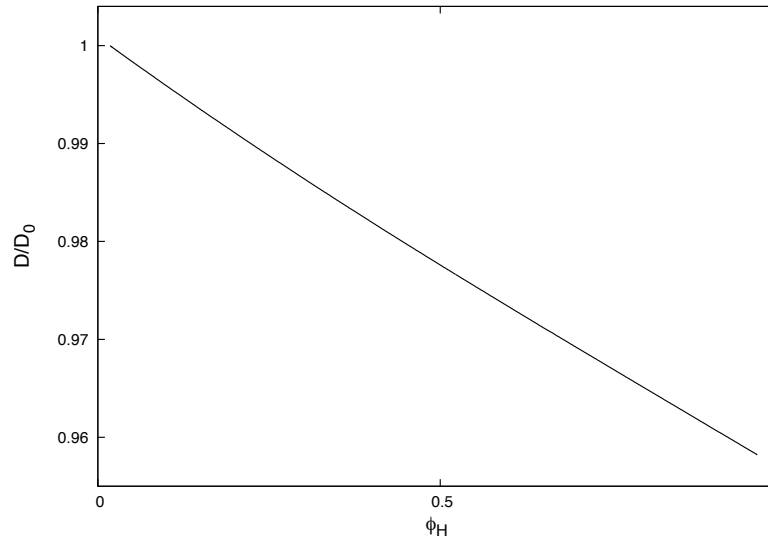


Figure 5.15: Normalized lamellar spacing for the $AB/A'B$ system with $\chi_{AB} = 13$ and $\xi_{A'}=1.25$.

chains are longer than the chemically identical A chains. It is also interesting to point out that the increase in the $A'B'$ concentration results in an increase in the A and

A' segment lengths. In contrast, B and B' segment lengths decrease with increase in the $A'B'$ concentration. Having analyzed the relative segment changes for all species, it can be firmly stated that the overall decrease in the lamellar spacing is caused by shrinking of the B and B' chains toward the lamellar interface.

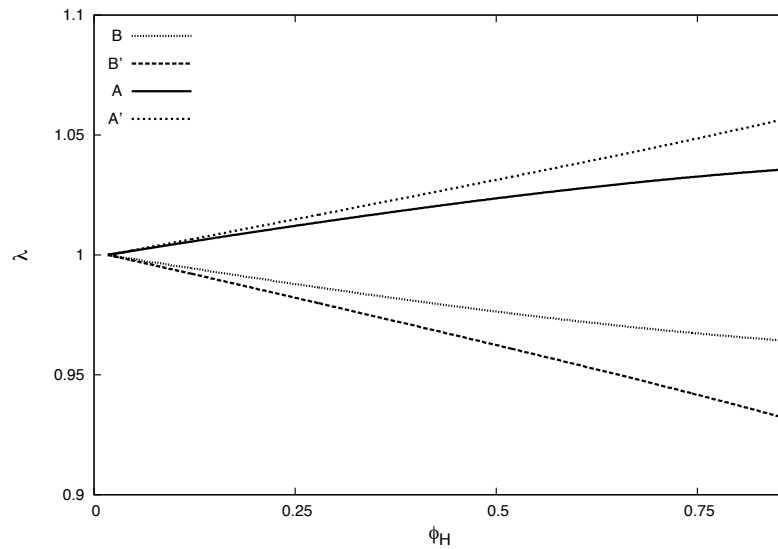


Figure 5.16: Normalized segment length for the $AB/A'B'$ system, where λ represents the length of each segment, normalized to its initial value.

This effect can be better understood by analyzing the schematic diagram shown in Fig[5.17]. Figure [5.17 a] shows a pure AB blend, in which none of the A chains have complexed. Increasing the homopolymer concentration results in the complexation of the A and C chains. This increases the $A'B'$ concentration in the system. As shown previously in Fig[5.16], the length of the A and A' chains increases, while

B and B' chains coil towards the interface. The overall result is a decrease in the lamellar spacing, as shown in Fig[5.17 c].

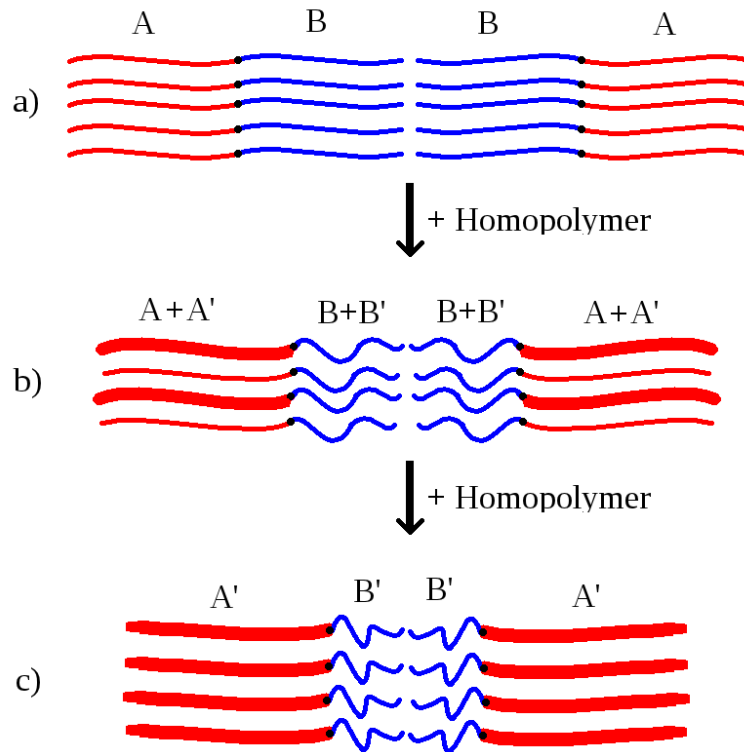


Figure 5.17: A schematic diagram showing the increase in the lamellar spacing with increase in the $A'B'$ concentration. a) Shows a pure AB blend, b) a blend with mixed $AB/A'B'$ and c) a pure $A'B'$ blend. Increase in the $A'B'$ concentration results in a decrease in the overall lamellar spacing.

The shrinking of the B' chain towards the $A'B'$ interface can be better understood by analyzing the schematic diagram shown in Fig[5.18]. In this diagram, the shrinking

of the B' chain is accounted for by considering the overall volume occupied by the segments. Since the blend is incompressible, this volume must be conserved. Before complexation, Fig [5.18 a], the volumes occupied by each segment (A and B) are equal and can be calculated as,

$$\begin{aligned} V_\alpha &= N_\alpha v_\alpha \\ &= A_{\text{int}} \lambda_\alpha \end{aligned} \quad (5.31)$$

where v_α is the volume occupied by a monomer of type α . Here, λ_α and A_{int} are the height and interfacial area of the cylinders shown in Fig[5.18]. N_α in equation (5.31) is the number of α monomers, where $\alpha = A, B, A', B'$. The interfacial area (A_{int}) is shared between the volumes occupied by each segment. After complexation, Fig[5.18 b], the volume occupied by the complexed monomers increases, resulting in an increase in the interfacial area. The increase in A_{int} means that λ_B must decrease to conserve the volume occupied by the B' monomers. This effect can be seen explicitly in Fig[5.16].

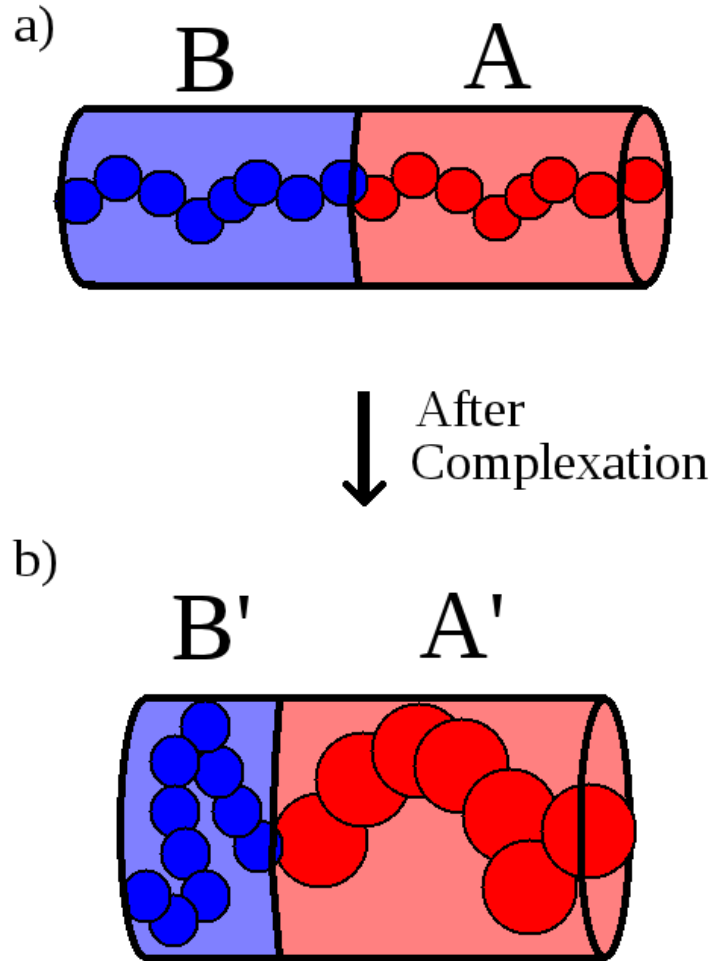


Figure 5.18: A schematic diagram showing the shrinking of the B' chain towards the interface. a) The volume occupied by each segment is equal before the complexation. b) The volume occupied by the A' segment increases, thus increasing the interface area. To conserve the volume, the B' segment coils towards the $A'B'$ interface. The interface between the volume occupied by the $A - B$ and $A' - B'$ is assumed to be circular for simplicity. The height of each cylinder is represented by λ_α .

Chapter 6

Summary and Conclusion

In this thesis, two models were introduced and investigated for describing hydrogen-bonding in AB diblock copolymer/ C homopolymer blends. In the first approach, hydrogen-bonding between the A and C monomers was modeled by a negative (attractive) interaction parameter. Phase diagrams in the f_A - ϕ_H and χ_{AC} - ϕ_H planes were constructed and found to be in qualitative agreement with experiments.¹⁰ The phase behavior in the χ_{AC} - ϕ_H plane was found to be sensitive to the hydrogen-bonding strength. Increasing the homopolymer concentration was shown to result in order-order phase transition of type Lam \rightarrow Hex \rightarrow BCC \rightarrow Dis, for large negative χ_{AC} values. Increasing ϕ_H for $\chi_{AC} \lesssim -2$ resulted in macrophase separation. The effect of hydrogen-bonding on the lamellar phase was further investigated by examining the lamellar domain spacing as a function of the homopolymer concentration. The attractive interaction model predicts an increase in the lamellar spacing for strong and weak hydrogen-bonding. This was shown to be caused by aggregation of the C monomers at the A rich domains of the lamellar phase. The increase in the lamellar spacing for weak hydrogen-bonding was found to be consistent with experiments.

In contrast, increase in the homopolymer concentration for strong hydrogen-bonding was observed experimentally to decrease the lamellar spacing.¹⁰ This disagreement between this model and the experiments indicates that hydrogen-bonding can not be correctly modeled by a negative interaction parameter.

In the second approach, interpolymer complexation was used to model hydrogen-bonding in the AB/C blend. The complexation model assumes a donor/ acceptor relationship between monomers with hydrogen-bonding capability. By analyzing the homogenous equilibrium state in the strong hydrogen-bonding regime, it was shown that the $AB+C \rightleftharpoons A'B'C'D$ complexation can be simplified as an $AB+C \rightleftharpoons B'D$ for strong hydrogen-bonding. This indicates that the majority of the reactions, result in a complete complexation between the A and C segments. The phase behavior of the $AB/B'D$ blend was found to be sensitive to the chain thickness of the complexed D monomers. The phase diagram in the ξ_D - ϕ_H plane showed an order-to-disorder phase transition for $\xi_D \gtrsim 1.5$. Using SCFT it was found that increase in ϕ_H for blends with $\xi_D = 2$ results in Lam \rightarrow Hex \rightarrow BCC \rightarrow Dis phase transitions. The phase sequence captured here is in agreement with experiments.¹⁰ The change in the lamellar spacing with respect to the homopolymer concentration was also investigated, where increase in ϕ_H was shown to result in a decrease in the lamellar spacing. This effect was further studied by considering an $AB/A'B'$ blend, with $\xi_{A'}=1.25$. Decrease in the lamellar spacing was found to be the result of the single-stranded B and B' chains coiling in towards the interface.

The analysis of the attractive interaction and interpolymer complexation models

indicate that hydrogen-bonding between polymer segments should be described by interpolymer complexation. It was shown that the phase behavior and the decrease in the lamellar spacing is caused by the increase in the volume occupied by the complexed chains. A more complete interpolymer complexation model can be constructed by considering changes to the hydrogen-bonding strength. In a such model, the complexation reaction would depend on the enthalpic and entropic contributions to the free-energy.

Although this thesis provided us with a good foundation for understanding hydrogen-bonding in polymer blends, more in-depth studies are required. In future work, we hope to extend the interpolymer complexation model to investigate the effect of hydrogen-bonding strength on the phase behavior of the AB/C system. In such a model, the concentration of the complexed chains is adjusted for locally, by calculating the mass action formalism. We also hope to study the effect of chain architecture on the phase behavior and develop a more realistic model for hydrogen-bonding systems.

Bibliography

1. I. Hamley, *Developments in block copolymer science and technology*. J. Wiley, 2004.
2. M. W. Matsen, “Phase behavior of block copolymer/homopolymer blends,” *Macromolecules*, vol. 28, no. 17, pp. 5765–5773, 1995.
3. A. N. Semenov, “Phase equilibria in block copolymer-homopolymer mixtures,” *Macromolecules*, vol. 26, no. 9, pp. 2273–2281, 1993.
4. J. Zhou and A.-C. Shi, “Microphase separation induced by differential interactions in diblock copolymer/homopolymer blends,” *The Journal of Chemical Physics*, vol. 130, no. 23, p. 234904, 2009.
5. Y. Zhuang, L. Wang, and J. Lin, “Hierarchical nanostructures self-assembled from diblock copolymer/homopolymer blends with supramolecular interactions,” *The Journal of Physical Chemistry B*, vol. 115, no. 23, pp. 7550–7560, 2011.
6. K. Dobrosielska, S. Wakao, J. Suzuki, K. Noda, A. Takano, and Y. Matsushita, “Effect of homopolymer molecular weight on nanophase-separated structures of ab block copolymer/c homopolymer blends with hydrogen-bonding interactions,” *Macromolecules*, vol. 42, no. 18, pp. 7098–7102, 2009.

7. M. Park, C. Harrison, P. M. Chaikin, R. A. Register, and D. H. Adamson, "Block copolymer lithography: Periodic arrays of 1011 holes in 1 square centimeter," *Science*, vol. 276, no. 5317, pp. 1401–1404, 1997.
8. S.-W. Kuo, "Hydrogen-bonding in polymer blends," *Journal of Polymer Research*, vol. 15, pp. 459–486, 2008.
9. N. Hameed, N. V. Salim, and Q. Guo, "Microphase separation through competitive hydrogen bonding in self-assembled a-b-b/c diblock copolymer/homopolymer complexes," *The Journal of Chemical Physics*, vol. 131, no. 21, p. 214905, 2009.
10. S.-C. Chen, S.-W. Kuo, U.-S. Jeng, C.-J. Su, and F.-C. Chang, "On modulating the phase behavior of block copolymer/homopolymer blends via hydrogen bonding," *Macromolecules*, vol. 43, no. 2, pp. 1083–1092, 2012/02/10 2009.
11. N. Hameed, J. Liu, and Q. Guo, "Self-assembled complexes of poly(4-vinylphenol) and poly(ϵ -caprolactone)-block-poly(2-vinylpyridine) via competitive hydrogen bonding," *Macromolecules*, vol. 41, no. 20, pp. 7596–7605, 2008.
12. K. Dobrosielska, S. Wakao, J. Suzuki, K. Noda, A. Takano, and Y. Matsushita, "Effect of homopolymer molecular weight on nanophase-separated structures of ab block copolymer/c homopolymer blends with hydrogen-bonding interactions," *Macromolecules*, vol. 42, no. 18, pp. 7098–7102, 2009.
13. H.-F. Lee, S.-W. Kuo, C.-F. Huang, J.-S. Lu, S.-C. Chan, C.-F. Wang, and F.-C. Chang, "Hydrogen-bonding interactions mediate the phase behavior of an

- ab/c block copolymer/homopolymer blend comprising poly(methyl methacrylate-b-vinylpyrrolidone) and poly(vinylphenol),” *Macromolecules*, vol. 39, no. 16, pp. 5458–5465, 2006.
14. K. Dobrosielska, S. Wakao, A. Takano, and Y. Matsushita, “Nanophase-separated structures of ab block copolymer/c homopolymer blends with complementary hydrogen-bonding interactions,” *Macromolecules*, vol. 41, no. 20, pp. 7695–7698, 2008.
 15. S. H. Han, J. K. Kim, V. Pryamitsyn, and V. Ganesan, “Phase behavior of binary blends of block copolymers having hydrogen bonding,” *Macromolecules*, vol. 44, no. 12, pp. 4970–4976, 2012/02/10 2011.
 16. B. Loewenhaupt, A. Steurer, G. P. Hellmann, and Y. Gallot, “Microphases and macrophases in polymer blends with a diblock copolymer,” *Macromolecules*, vol. 27, no. 4, pp. 908–916, 1994.
 17. I. Nakamura and A.-C. Shi, “Phase separation induced by ladder-like polymer-polymer complexation,” *The Journal of Physical Chemistry B*, vol. 115, no. 12, pp. 2783–2790, 2011.
 18. W. B. Lee, R. Elliott, K. Katsov, and G. H. Fredrickson, “Phase morphologies in reversibly bonding supramolecular triblock copolymer blends,” *Macromolecules*, vol. 40, no. 23, pp. 8445–8454, 2007.
 19. E. H. Feng, W. B. Lee, and G. H. Fredrickson, “Supramolecular diblock copolymers: a field-theoretic model and mean-field solution,” *Macromolecules*, vol. 40, no. 3, pp. 693–702, 2007.

20. G. Fredrickson, *The Equilibrium Theory of Inhomogeneous Polymers*, ser. International Series of Monographs on Physics. Clarendon Press, 2006.
21. T. Kawakatsu, *Statistical Physics of Polymers: An Introduction*, ser. Advanced Texts in Physics. Springer, 2004.
22. J. Sakurai and S. Tuan, *Modern Quantum Mechanics*. Addison-Wesley Publishing Company, 1994.
23. K. Lee and S. Kobayashi, *Polymer Materials: Block-Copolymers, Nanocomposites, Organic/Inorganic Hybrids, Polymethylenes*, ser. Advances in Polymer Science. Springer, 2010.
24. L. Leibler, “Theory of microphase separation in block copolymers,” *Macromolecules*, vol. 13, no. 6, pp. 1602–1617, 1980.
25. E. W. Cochran, D. C. Morse, and F. S. Bates, “Design of abc triblock copolymers near the odt with the random phase approximation,” *Macromolecules*, vol. 36, no. 3, pp. 782–792, 2003.
26. J. Boyd, *Chebyshev and Fourier Spectral Methods*, ser. Dover books on mathematics. Dover Publications, 2001.
27. H. Wang and M. Anderson, *Introduction to Groundwater Modeling: Finite Difference and Finite Element Methods*. Elsevier Science, 1995.
28. I. Gladwell and R. Wait, *A Survey of numerical methods for partial differential equations*. Clarendon Press, 1979.

29. M. W. Matsen and M. Schick, “Stable and unstable phases of a diblock copolymer melt,” *Physical Review Letters*, vol. 72, no. 16, pp. 2660–2663, 04 1994.
30. J. Strikwerda, *Finite Difference Schemes And Partial Differential Equations*. Society for Industrial and Applied Mathematics, 2004.
31. Z. Li and K. Ito, *The Immersed Interface Method: Numerical Solutions of PDEs Involving Interfaces And Irregular Domains*, ser. Frontiers in Applied Mathematics. SIAM, Society for Industrial and Applied Mathematics, 2006.